8-1-2016

Structural Evolution of the Maynard Lake Fault Within the Left-Lateral Pahranagat Shear Zone, Nevada, USA

Mahmud Mustafa Muhammad
University of Nevada, Las Vegas, mahmud.geology@gmail.com

STRUCTURAL EVOLUTION OF THE MAYNARD LAKE FAULT WITHIN THE LEFT-LATERAL PAHRANAGAT SHEAR ZONE, NEVADA, USA

By

Mahmud Muhammad

Bachelor of Science in Geology
Salahaddin University-Erbil, Kurdistan Region-Iraq
2010

A thesis submitted in partial fulfillment
of the requirements for the

Master of Science – Geoscience

Department of Geoscience
College of Sciences
The Graduate College

University of Nevada, Las Vegas
August 2016

UNLV | GRADUATE COLLEGE

Thesis Approval

The Graduate College
The University of Nevada, Las Vegas

May 19, 2016

This thesis prepared by

Mahmud Muhammad

entitled

Structural Evolution of the Maynard Lake Fault Within the Left-Lateral Pahranagat Shear Zone, Nevada, USA

is approved in partial fulfillment of the requirements for the degree of

Master of Science – Geoscience
Department of Geoscience

Wanda J. Taylor, Ph.D.
Examination Committee Chair

Kathryn Hausbeck Korgan, Ph.D.
Graduate College Interim Dean

Pamela Burnley, Ph.D.
Examination Committee Member

Ganqing Jiang, Ph.D.
Examination Committee Member

Barbara Luke, Ph.D.
Graduate College Faculty Representative

ABSTRACT

STRUCTURAL EVOLUTION OF THE MAYNARD LAKE FAULT (MLF) WITHIN THE LEFT-LATERAL PAHRANAGAT SHEAR ZONE (PSZ), NEVADA, USA

By

Mahmud Muhammad

Dr. Wanda J. Taylor, Examination Committee Chair

Professor of Geoscience

University of Nevada, Las Vegas

The Pahranagat shear zone (PSZ) contains three ENE-striking left-lateral strike-slip faults: The Arrowhead Mine fault (AMF), Buckhorn fault (BF), and Maynard Lake fault (MLF) from north to south. This shear zone lies along the boundary between the northern and central Basin and Range physiographic sub-provinces (NBR-CBR). In addition, this zone is positioned SW of a regional strike-slip zone, the Caliente-Enterprise zone (CEZ), and surrounded by extensional domains with differences in timing and magnitude of extension. Hence, understanding the development of the PSZ, particularly the MLF, is essential to better understanding tectonic evolution of the boundary zone between the northern and central Basin and Range including the formation of strike-slip zones, geometry of structures, timing of deformation, and kinematic history.

The knowledge of structural development of the western MLF, which has the largest offset of all faults within the PSZ, is needed to increase the understanding of the development of a major

strike-slip zones within the NBR-CBR boundary. Key aspects in the development include the timing of deformation, heterogeneous deformation along strike-slip zones such as strike-slip duplex formation, and possibility of strain transfer locally between faults and regionally between extensional domains. The western extent of the MLF, geometry of the MLF, and occurrence of reverse faults within the MLF zone were unclear prior to this study. In this study, a new 1:12000 scale map of the western MLF and northwestern part of the Sheep Range provides data on the formation of strike-slip zones, timing of deformation, kinematic history, and geometry of structures.

I used a well-documented regional stress field measurement for the area, as well as my own observations of fault strike orientation, map cross-cutting relationships, the attitude of beds and compaction foliations from ash-flow tuffs, and contractional features such as folds, to analyze the kinematic compatibility and timing of deformation for the PSZ including the MLF zone. The data and analysis show that the MLF is a sinistral strike-slip fault that transfers strain between two extended regions separated by a less extended region south of the MLF. This transfer zone, the PSZ and MLF, represents the SW continuation of the larger strike-slip zone, CEZ, in the vicinity of the NBR-CBR boundary. In addition, at least three stages of deformation were documented for the MLF zone; (1) Pliocene to Quaternary (2) middle-Miocene to Pliocene (3) early-middle Miocene.

Keywords: Maynard Lake Fault, Pahranagat Shear Zone, Strike-slip duplex, Apparent Reverse Faults, Extensional Tectonics, Timing of deformation.

ACKNOWLEDGEMENTS

The success of this project was achieved by the persistent hard work and great support from my family, my academic advisor, friends, coworkers, organizations and institutions that I have worked with. I am honored to have them in my life and I will use this opportunity to express my sincere gratitude to each of them below.

First, thanks to God that surrounded me with such kind people in my life. Thanks to my beloved family in Kurdistan. A special thanks to Dr. Wanda Taylor for her continuous support, encouragement and the knowledge she passed to me. I will make sure to deliver and pass this valuable knowledge and experience to my future students. Also, I am thankful to my committee members Dr. Barbara Luke, Dr. Ganqing Jiang, and Dr. Pamela Burnley for their supportive and valuable comments and feedback.

Also, I would like to thank all the organizations and institutions that funded my stay in the USA, and my master's thesis project. Thanks to Exxon-Mobil and Institute of International Education for providing me a unique scholarship that funded both non-academic (language preparation) and academic (Master's program) over the last three years. I appreciate the time and effort of my scholarship advisors Laila Agily, David DeGroot and Selene Escalera; your support made my life so much easier. Also, thanks to the following organizations that supported my field work expenses; U.S. Geological Survey EDMAP program award G15AC00157 to W.J. Taylor and Nevada Petroleum and Geothermal Society. Thanks to University of Nevada Las Vegas for creating such a peaceful environment for students. Thanks to students and faculty members at the Geoscience Department for having me as a friend during the last two years. Particularly, thanks to the faculty members and professors for sharing their knowledge through classes and during geologic field trips.

Thanks to my field assistants, Jeffery Kinney, Jeremey Miera, and Alexander Peck. Also, thanks to friends and colleagues Chant Kazanjian, Michael Evans, Shaima Abdulhaleem, Thomas Price, Alexander Peck, Lauren Parry, and Amanda Gentry.

DEDICATIONS

To my parents, who taught me to be kind, generous and always eager to sacrifice!

To my beloved mother who never been a student at schools, but because of her I have had access to school education!

To all of my teachers who taught me from kindergarten to graduate school!

TABLE OF CONTENTS

LIST OF FIGURES

CHAPTER 1

INTRODUCTION

The Basin and Range province (BRP) in western North America contains four sub-provinces: Northwestern, Northern, Central, and Southern (NWBR, NBR, CBR, and SBR) (Fig. 1) (Jones et al., 1992; Wernicke 1992; Sonder and Jones, 1999; Colgan et al., 2004, 2006; Hammond and Thatcher, 2005). The sub-provinces differ in basin elevations such that the NBR has the highest basin elevation, and the SBR has the lowest. The boundary between the NBR and CBR is indicated by anomalies in gravity, differences in patterns of magmatism (Figs. 2 and 3), and particularly a transition between a zone of no surface volcanism and a zone with volcanism (Fig. 3). In addition, the local correlation between magmatism and extension is poor (Taylor et al., 1989; Axen et al., 1993; Liu, 1996). This boundary also is marked by caldera complexes and left-lateral fault zones, one of which is the Paharanagat shear zone (PSZ) (Figs. 1 and 4). Furthermore, the NBR-CBR boundary accommodates a regional strike-slip zone including the Caliente-Enterprise zone (CEZ) (Jayko, 1990; Axen, 1998). Understanding the sub-province boundary development, in particular the PSZ, will aid in further characterizing the regional tectonic development of the BRP.

The timing of the initiation of extension and its spatial distribution in the sub-provinces vary, which also suggests the presence of rift segment boundaries between them. In the NWBR at the latitude of Oregon extension began about 15 Ma (Colgan et al., 2004, 2006; Hammond and Thatcher, 2005); in the NBR, Oligocene-Miocene regional extension began about 40 to 30 Ma, in the Southern Basin and Range (SBR) about 25 Ma; and in the Central Basin and Range (CBR) about 18 to 13 Ma (Axen et al., 1993; Sonder and Jones, 1999 and references therein; Anderson and Beard, 2010; Bidgoli et al., 2015). In addition, in the northeastern part of the NBR, some

areas extended during Cretaceous to Eocene overall contraction (e.g., Wells et al., 2012). Extension in the SBR migrated from the south toward the CBR (Sonder and Jones, 1999) and extension in the NBR began in two N-S oriented belts (Axen et al., 1993). In contrast, extension in the CBR initiated and occurred across the entire width of the Basin and Range during a short time interval in post middle Miocene time (Wernicke, 1992).

The boundary zone between the NBR and CBR (Fig. 1) encompasses the PSZ, which includes three major northeast-striking, left-lateral strike-slip faults: The Arrowhead Mine, Buckhorn, and Maynard Lake faults (MLF) (Fig. 4), and two caldera complexes. This shear zone was first mapped by Tschanz and Pampeyan (1970). These three post-early Miocene faults have a total apparent offset as great as 15 km (Liggett and Ehrenspeck, 1974; Jayko, 2007). Ekren et al. (1977) confirmed the post- early Miocene movement of the PSZ. To date, studies have not documented pre-Tertiary extension within the PSZ (e.g., Jayko, 1990; Taylor and Bartley, 1992; Axen et al., 1993; Scott et al., 1995; Switzer and Taylor, 2001; this study).

The motivation behind conducting research on the PSZ, particularly the left-lateral strike-MLF, stems from the location of this structure along the boundary between NBR and CBR (Fig. 1). Documenting the geometry, kinematics and timing of deformation along the PSZ, especially the MLF, will place constraints on the development of the boundary zone. The recently published geologic map (1:100,000; Jayko, 2007) lacks the detail to provide these constraints; particularly, existing map relations are unclear about whether the MLF bends southwest along the western Sheep Range or continues WSW toward the Desert Range.

This paper has five goals to investigate the MLF, the longest fault in the PSZ. 1. Ascertain a left-lateral motion for the PSZ including the MLF zone. Previous studies suggested a lefl-lateral motion for the PSZ and the MLF due to the apparent offset of units and slickenlines exposed at

the eastern part of the MLF; however, the continuation and sense of movement is poorly known west of the PSZ and the MLF zone.

2. Whether the MLF bends, ends or splays in the northwestern Sheep Range will determine how strain is distributed along the NBR-CBR boundary. Previous work suggested that the MLF may either bend southwest along strike from a NE-strike in the northern Sheep Range to N-strike along the western Sheep Range or the MLF may continue westward from the western Sheep Range toward the Desert Range (Tschanz and Pampeyan, 1970; Ekren et al., 1977). Constraining whether the MLF bends or splays is essential to understand and model the distribution of strain and the deformation style such as simple shear, pure shear or a combination of both.

3. The geometry and style of deformation along the western end of the MLF was examined to evaluate how local contractional structures are related to the formation of a duplex structure within the current strike-slip system. Byron (1995) recognized contractional structures along the northeastern part of the MLF and found that these structures are coeval with strike-slip faulting and normal faulting. However, she has not explained the geometry and cause of these local contractional features.

4. Defining the structural geometry and kinematics of the PSZ contributes to understanding the development of the Basin and Range sub-province boundaries. The PSZ lies southwest of a major strike-slip zone, CEZ, within the NBR-CBR boundary. Therefore, the structural geometry and kinematics of the PSZ can constrain the southwest boundary of a major strike-slip zone, CEZ, within the NBR-CBR sub-province boundaries. Constraining the timing of deformation, as part of the kinematics, is essential to understanding how extension correlates to magmatism in the region, in particular within the PSZ and NBR-CBR boundary.

5. Documenting the detailed location of young fault scarps along the MLF is critical to understanding the Quaternary tectonics and seismic hazards. This zone previously was suggested to transfer motion from the Wasatch fault zone to the Eastern California Shear zone (Kreamer et al., 2010) (Fig.5). Therefore, understanding the Quaternary deformation within the PSZ and MLF may aid in mitigation of seismicity threats to the people living in Alamo and the Las Vegas area.

This master's thesis is part of a bigger project, along with master's theses research by two of my colleagues Michael Evans and Thomas Price. The larger project includes mapping the entire Lower Paharanagat Lake NW 7.5' quadrangle and surrounding area of the PSZ at 1:12000 scale; to better document the boundary zone between the NBR and CBR sub-provinces.

I used the documented regional stress field for the area (e.g., Zoback, 1989), fault strike orientation, mapped cross-cutting relationships, the attitude of beds and compaction foliations from volcanic rocks, and contractional features such as folds, to determine the kinematic compatibility and timing of deformation for the PSZ, particularly the MLF zone. The data show that the MLF is a sinistral strike-slip fault that transfers strain between two extended regions separated by a less extended region north of the Sheep Range. In addition, at least three stages of deformation were documented for the MLF zone; (1) Pliocene-Quaternary (2) latest Miocene-Pliocene (3) early-middle Miocene; suggesting that deformation occurred late in the sub-province boundary development.

CHAPTER 2

GEOLOGIC SETTING

The rocks in the NBR-CBR boundary zone experienced multiple deformations since Jurassic. These deformations include Mesozoic shortening and Cenozoic extension. This boundary zone is largely superimposed on the shortening structures and developed during Cenozoic extension. Marked Cenozoic geologic differences occur across the boundary.

JURASSIC TO CRETACEOUS SHORTENING

The western United States experienced various orogenies that caused the formation of fold and thrust belts from late Devonian until about the Eocene**.** The Jurassic-Eocene Sevier orogeny structures are well known in south and east-central Nevada. The Gass Peak thrust, which correlates to the Golden Gate-Mount Irish thrust and the rest of the Garden Valley thrust system are Sevier orogeny structures within the vicinity of the NBR-CBR boundary (Taylor et al., 2000). The northward correlation of the Gass Peak thrust with the Pahranagat and Golden-Gate-Mount Irish thrusts is consistent with a left-lateral offset of the Paharanagat shear zone (Taylor et al., 2000).

Extensive Tertiary deposits, mainly Oligocene-Miocene ignimbrites unconformably overlie the fold and thrust belt and aid in reconstructions (e.g., Long, 2012). The post Oligocene offset of the volcanic rocks is overprinted on the folds and thrusts (Taylor et al., 2000) and must be removed to restore and correlate the older structures. Determining which structures are overlain by the ignimbrites and which structures cut them allows structures to be temporally distinguished.

LATE CRETACEOUS TO EOCENE EXTENSION

At the end of the Sevier and the Laramide orogenies, which over thickened the western North American crust, roll back of the shallowly subducted oceanic slab underneath the Northern American plate caused a switch to normal subduction and back arc extension at about 50-20 Ma (Atwater, 1971; Zoback et al., 1981; Stewart, 1998; Dickinson, 2006). This switch of subduction angle was most probably caused by the delamination of the previously subducted flat slab and/or changes in mantle flow. The late Cretaceous to Eocene extension is attributed to gravitational collapse as a response to the over thickened crust or lithospheric delamination (Sonder and Jones, 1999; Liu, 2001; Wells et al., 2012). In the NBR, Late Cretaceous extension is documented in northeastern Nevada, northwestern Utah, and southeastern Idaho within the Pequop, Raft River, and Black Pine Mountains (Camilleri, 1997; Wells et al., 2012), however, extension did not appear within the Pahranagat area until about Late Eocene (Axen et al., 1993; Scott et al., 1995; Taylor and Switzer, 2001).

OLIGOCENE AND MIOCENE EXTENSION

NORTHERN BASIN AND RANGE

In general, four stages of extension are suggested for the NBR within Nevada and close to the Paharanagat area, although only the last two stages may appear within the Paharanagat area (e.g., Taylor and Bartley, 1992; Axen, 1993; Scott et al., 1995; Switzer and Taylor, 2001). The stages are as follows: 1. Pre-32 Ma extension identified from the accumulation of thick pre-late Oligocene conglomerate and lacustrine limestone suggests a pre-volcanic extension for the Dry Lake area in the North Pahroc Range, northeast of the PSZ (Fig. 6). 2. An early mild syn-volcanic extension at about 30 Ma to 27 Ma (Taylor et al., 1989) is supported by angular unconformities within the Oligocene ash-flow tuff sequence within the North Pahroc Range. 3.

The peak extension during 22 Ma to 12 Ma is associated with stratal tilting and detachment faults (Axen, 1993; Anderson et al., 2010) and strike-slip, oblique-slip and high-angle normal faulting (Scott et al., 1995). 4. The last stage is the post 10-Ma extension that defined the current Basin and Range topography (Anderson et al., 1983).

The 34-17 Ma voluminous volcanic eruptions in the NBR, which are called the ignimbrite flare-up, indicate that there should be a strong mantle upwelling prior to extension (Liu and Shen, 1998). Sonder and Jones (1999) attributed the NBR extension to the combination of potential energy forces originated from crustal thickening and asthenospheric upwelling. The role of asthenospheric upwelling is not simple in this extension because the timing relations between extension and volcanism vary. The NBR extension in some places precedes volcanism, for example, >70 km to the north and northeast of the PSZ along the Snake-Stampede detachment system, which consists of the Snake Range decollement, Stampede detachment and Seaman breakaway fault (Taylor and Bartley, 1992; Axen et al., 1993). In contrast, the syn-volcanic extension is identified north of the PSZ within the North Pahroc, Golden Gate, Hiko and Highland Peak ranges (Taylor and Switzer, 2001). Post-volcanic extension is documented regionally, such as within the Hiko Range, western Timpahute Range, and within and around the Meadow Valley southeast of the Pahranagat shear zone (Axen et al., 1993; Scott et al., 1995; Switzer and Taylor, 2001).

Volcanism within the NBR sub-province swept southward through time (Sonder and Jones, 1999; Henry, 2008; Best et al., 2013a, b). The major phase of volcanism within this part of the northern Basin and Range did not start until about Late Eocene-Oligocene (Best et al., 1993; Best et al., 2013 a and b). The southward sweep of volcanism ends approximately at the latitude of 37^{o} N to 36^{o}N around the PSZ.

The PSZ is surrounded by caldera complexes: the centers of the Southern Nevada volcanic field to the west, Central Nevada caldera complex to the north, Caliente and Indian Peak caldera complexes to the east; and Kane Springs Wash caldera to the southeast. The tuffs within and near the PSZ mainly originated from the Central Nevada and Caliente-Indian Peak caldera complexes. The radiometrically dated tuffs of the Central Nevada caldera complex have ages between 36.1 Ma and 18.57 Ma (Best and Christiansen, 1991; Best et al., 2013a and b) and the radiometrically dated tuffs which erupted from the Caliente and Indian Peak caldera complexes have ages between 36.2 Ma and 18.1 Ma (Best and Christiansen, 1991; Best et al., 2013 a and b). In addition, the 14.5 Ma Kane Springs Wash Tuff (Best and Christiansen, 1991; Best et al., 2013a and b) is deposited within the PSZ. The Kane Springs Wash Tuff does not appear at the northwestern end of the Sheep Range or in the mapped area. The current (Plate 1, Fig. 6) and previous geologic maps (Jayko, 2007; Price, in progress MS thesis; Evans, in progress MS thesis) of the Pahranagat area including the PSZ show deformation of tuffs as young as 14.5 Ma and tuffs as old as 27.57 Ma. Therefore, exposed extension within the PSZ must be middle Miocene or younger.

The direction of least principal stress has changed a few times since the Eocene within the NBR (Zoback et al., 1981; Best, 1988; Zoback, 1989; Taylor and Switzer, 2001). The direction of least principal stress changed from NNW to ENE at about 50 Ma to 30 Ma, but the timing of this change was not synchronous for the entire western United States (Best, 1988). The change of the least principal stress direction started first in the southeastern part of the western United States and swept toward the northwestern of the western United States (Best, 1988). For almost the entire Oligocene a NNW least principal stress direction is documented (Zoback et al., 1981; Best, 1988). During the Late Oligocene- Early Miocene, a NW to NE direction of least principal

stress is identified; furthermore, a N to E with an average ENE direction is identified for the entire Miocene (Zoback et al., 1981; Best, 1988; Axen, 1993; Switzer and Taylor 2001). Additionally, during volcanism a 90^{o} change is suggested, at least locally, for the direction of least principal stress within the NBR (Best and Christiansen, 1991; Switzer and Taylor, 2001; Bidgoli**,** 2005).

Rowley (1998) suggested that most transverse zones act as boundaries separating zones of a different style, amount, and rate of strain. In other words, they are accommodation zones and/or transfer faults. Moreover, related extensional faults are commonly bounded by transverse zones. The NBR is well known to have major transverse zones, one of which is the CEZ or Escalante zone. The Paharanagat shear zone has been suggested to form the western part of the CEZ (Axen, 1998). Transverse zones and the CEZ including the Pahranagat Shear Zone are further discussed below.

CENTRAL BASIN AND RANGE

The Central Basin and Range extension south of the PSZ is defined by two major zones of Neogene extension of the upper crust: The Lake Mead extended domain to the east and the Death Valley extended domain to the west (Wernicke, 1992; Wernicke and Snow, 1998). Approximately 50 km north of Lake Mead, and east and southeast of the Pahranagat and the Sheep ranges, the extended eastern domain includes three detachment faults: The Castle Cliffs, Tule Springs and Mormon Peak detachments (Fig. 6) (Bidgoli et al., 2015). The Castle Cliffs detachment lies at the eastern boundary of the CBR separating the highly extended region to the west from the relatively stable Colorado Plateau to the east. This detachment fault is the oldest among the three faults with footwall exhumation evident at 18-17 Ma (Bidgoli et al., 2015). The middle detachment fault, the Tule Springs detachment, appears in the Tule Springs Hills (Fig. 6).

The relative age of the Tule Springs detachment derived from the cross-cutting relationship between this fault and dated Tertiary volcanic rocks suggests that the Tule Springs detachment was active from the middle to late Miocene (Axen, 1993; Bidgoli et al., 2015). The Mormon Peak detachment must be active at least no earlier than late Miocene. Recent data (Bidgoli et al., 2015) suggests that the Mormon Peak detachment was active since 14 Ma. The onset of extension among the above mentioned detachment faults decreases from east to west (Bidgoli et al., 2015).

The area north of the Mormon Mountains, prior to 23 Ma, was the site of lacustrine deposition. Afterwards, the southward migration of volcanism destroyed the lake environment (Anderson et al., 2010). Between 24 Ma and 17 Ma, a block to block change in stratigraphy might indicate an early stage of deformation; in addition, about 45^{o} of easterly tilting of blocks followed the deposition of the basin assemblage after 14 Ma.

In the Kane Wash area (Fig. 6), east of the Sheep Range and the PSZ, variations in distribution, degree, style, and timing of deformation demonstrate heterogeneous extension (Scott et al., 1995). In addition, approximately 55^{o} of progressive tilting of the Oligocene-Miocene volcanic units is documented to the area northeast of the Kane Wash caldera and north of the Meadow Valley Mountains (Scott et al., 1992).

The above three detachment faults, Castle Cliff, Tule Springs and Mormon Peak, are located in an area east of an east-trending zone of magmatic gap or amagmatic zone (Anderson et al., 2010; Rau and Forsyth, 2011). This amagmatic zone formed between the southward sweep of magmatism from the NBR and the northward sweep of magmatism from the SBR (Axen et al. 1993; Anderson et al., 2010; Rau and Forsyth, 2011). Despite the fact that the amagmatic zone refers to a zone of no volcanism, it is surrounded by active and young volcanism like the Coso

volcanic field to the west (Rau and Forsyth, 2011). Rau and Forsyth (2011) suggested that the amagmatic zone and CBR might have melt at depth, but it is expected to be trapped by the low-angle normal faults (e.g., Castle Cliff, Tule Springs and Mormon Peak detachments) which limited surface volcanism.

The extended western zone of the CBR, southwest of the PSZ, lies in the area between the mildly extended Spring Mountain block and the Sierra Nevada normal fault system (Wernicke, 1988; Wernicke and Snow, 1998). This zone, north of the Las Vegas Valley shear zone, and west of the Sheep Range, includes structures that accommodated extension and approximately 20^{o} eastward tilting of the Sheep Range as a result of three high-angle normal faults (Fig. 6) (Guth, 1981). This part of the CBR also has detachment faults like the Sheep Range detachment and Hoodoo Hills Havoc detachment (Guth, 1981). The area west of the Sheep Range extended about 100% since faulting started during the Miocene whereas the area south of the Las Vegas Valley shear zone did not extend significantly in the Miocene, and thus the Las Vegas Valley shear zone bounded the extending terranes on the south and acted as a transfer fault (Guth, 1981). In addition, extension within the area between the Las Vegas Range and the Desert Range is not associated with volcanism, intrusion or metamorphism (Guth, 1981).

The CBR is characterized by two major strike-slip fault zones; the Las Vegas Valley Shear Zone, and the left-lateral Lake Mead fault system. The Las Vegas Valley shear zone ends on the southeast where it reaches to the Lake Mead fault system. Both the Las Vegas Valley shear zone and the Lake Mead fault system are thought to have acted together and compensated the localized extension between the Colorado Plateau and the vicinity of the Specter Range to the west (Guth, 1981). In addition, recent work (Abdelhaleem, 2015) suggests that the Las Vegas Valley shear zone is deformed by younger structures which suggest that it is no longer active.

PLIOCENE-QUATERNARY EXTENSION

Quaternary faults within and around the PSZ at the boundary between the NBR-CBR sub-provinces were documented previously (U.S Geological Survey and Nevada Bureau of Mines and Geology, 2006). However, the spatial distribution and extent of many of these faults need closer attention. The activities of the Quaternary faults are essential to better understanding the seismicity of the region. The Quaternary faults south of the PSZ, in particular adjacent to the MLF, that may have related to the PSZ include the MLF, the Sheep Range fault, Sheep Basin fault, Sheep-East Desert Range fault, Coyote Spring fault, Arrow Canyon Range fault, Wildcat Wash fault, and Kane Spring Wash fault (Fig. 6). In addition, north of the PSZ the Quaternary faults include the unnamed faults of the Badger Valley, Tikaboo fault, Pahroc fault, Dry Lake fault, Delamar Mountains fault, and Delamar Valley fault (Fig. 6).

The spatial distribution of the Quaternary faults is essential to define different extensional boundaries. The Sheep Basin fault starts north of the Las Vegas shear zone right at the northern end of the Mormon Pass fault and extends toward the northwestern end of the Sheep Range (Guth, 1981; Guth, 1990; Anderson, 1999b). The southern portion of the Sheep Basin fault lies between the western base of Mule Deer Ridge and the western Sheep Range. The southwestern Sheep Range block, south of the Sheep Basin fault between the Mormon Pass fault and the Wilde Horse Pass fault dips an average of 20^{o} E (Fig. 6) (Guth, 1981). Contrastingly, the northwestern end of the Sheep Range adjacent to the northern part of the Sheep Basin fault dips average about 15^{o} east (Plate 1). This change in the dip of the rocks may be accommodated by heterogeneous slip along the Sheep Basin fault from the southwestern Sheep Range towards the northwestern end of the Sheep Range.

The Sheep Range fault lies east of the Sheep Basin fault and east of the Sheep Range. This fault strikes north and bounds the north and northwestern part of Coyote Valley. Extending toward the north, it probably intersects the east-northeast-striking MLF (Piety, 1996). The Sheep Basin fault and Sheep Range fault are suggested to strike north-northeast and north respectively. However, previously Piety (1996) and Anderson (1999b) suggested that the Sheep Basin fault veers into a northeast strike at the northwestern end of the Sheep Range; this study is in discordance with that. I suggest that the Sheep Basin fault may reactivate, cut or terminate into the MLF.

East and northeast of the Sheep Range fault is the Coyote Spring fault (Fig. 6). This north-striking fault extends north to the Delamar Mountains. This fault is considered to be a down-to-the west Basin and Range fault that splits the Delamar Mountains from the northern Sheep Range (Anderson, 1999c). Anderson (1999c) referenced to Schell (1981), suggested that this fault may merge with the Kane Spring Wash fault, which lies to the south.

South and southeast of the Coyote Spring fault is the Kane Spring Wash fault. The Kane Spring Wash fault is a sinistral northeast-striking fault and is suggested by Ekren et al. (1977) to be part of the PSZ. Harding et al. (1992) observed twenty faults including strands of the Kane Spring Wash fault and they measured slickenlines on the faults. Fifteen of the faults had components of strike-slip and five of the faults had pure-dip slip. Among the faults with strike-slip components eight of them show a normal left-lateral slip, however, a few faults have normal right-lateral slip (Harding et al. (1992). Furthermore, Harding et al. (1992) showed left-lateral offset of the Kane Springs Wash caldera, suggesting that the majority of slip along the Kane Springs Wash fault has a sinistral motion.

CALIENTE ENTERPRISE ZONE

Major east-trending lineaments have been mapped within the NBR such as Timpahute lineament, Pioche mineral belt, Delamar mineral belt, and CEZ (e.g., Ekren et al. 1976; Ekren et al. 1977; Jayko, 1990; Axen, 1998; Switzer and Taylor, 2001). These east-trending lineaments coincide with areas of lithologic boundaries, faults, caldera boundaries, ends of ranges and valleys, and magnetic interruptions (Ekren et al., 1976; Hudson et al., 1998; Rowley, 1998). The magnetic disruptions and anomalies along these lineaments can be related to the juxtaposition of different rocks by faulting and plutonic rock intrusions into structures along the lineaments (Ekren et al., 1976). The CEZ (Fig. 6), an east-northeast trending zone about 220 km long, interrupts north-south structures of the Basin and Range; this zone either lies directly NE of the PSZ or is continuous with the PSZ.

The CEZ (Fig. 6) is divided into three parts; eastern, central and western. This zone extends from the western boundary of the mildly extended Colorado Plateau to its western end at the PSZ. The eastern part lies along an east-west trending part of the Colorado Plateau margin; the central part coincides with the Caliente Caldera Complex, and the western part coincides with or ends at the PSZ (Axen, 1998).

The CEZ may have originated during late Eocene-early Oligocene extension at the boundary between the Stampede detachment system to the north and the inactivity to the south (Axen et al., 1993; Axen, 1998) (Fig. 6) or in the Miocene between areas of differential extension between the Highland detachment system and high angle normal faults to the north and the Mormon Peak-Tule Springs-Castle Cliff detachments to the south. The CEZ probably formed the southern boundary of a north trending extensional belt in the NBR (Axen et al., 1993; Axen, 1998). In addition, along the southwestern of the CEZ is a corridor of relatively low extension in the

Arrow Canyon Range, northern Sheep Range, southern Delamar Mountains, and Meadow Valley Mountains (Wernicke et al., 1988) (Fig. 6).

A transfer fault model was suggested for the CEZ including the Pahranagat Shear zone (Jayko, 1990, 2007; Hudson et al., 1998). Hudson et al. (1998), using paleomagnetic data, described and interpreted the orientation and variation of rotation in the CEZ; they suggested about 40 km of offset along the eastern Caliente-Enterprise zone, between a westward jog of the Colorado Plateau and a corridor of high extension in the eastern NBR to the north (Fig. 6). In general, rotation and tilting decreases from the east to the west along the CEZ. Within the central part of this zone, on the south between the Beaver Dam and Mormon Mountains (Fig. 6), sinistral offset decreases as a result of the large magnitude extension and, hence, it helps to reduce the rotation and tilting (Hudson et al., 1998). Similarly, farther west near the Kane Springs Wash fault zone and the PSZ (Fig. 6) rotation decreases as the offset is accommodated by discrete sinistral faults (Hudson et al., 1998).

CHAPTER 3

METHODOLOGY

About 35 km^2 around the southern PSZ including the western part of the MLF and the northwestern end of the Sheep Range mapped at 1:12000 scale to obtain spatial, geometric and kinematic data. Standard geologic field techniques using a Brunton compass, topographic base map, satellite imagery and hand lens were used in the field. Structural data including planar features such as bedding, compaction foliation and fault planes were measured using the Brunton compass. The Fieldmove-clino program was used as a portable field geodatabase to store the measured data from both compass and Fieldmove-clino.

Classic three-point problem calculations and the data-layer ArcMap tool, provided for free through personal communication with the authors (Kneissl et al, 2010), were used to calculate the fault attitudes. Field measurement data such as attitudes of compaction foliations and bedding as well as calculated structural data were used to construct cross-sections from the geologic map.

Stereonet techniques and software (Allmendinger et al., 2014) were used to plot the gathered structural data such as faults and folds to determine their orientation and validate the kinematic compatibility of the structures. Rose diagrams were constructed of compaction foliations from the different domains of the map area to understand the spatial change in the attitude of the units.

CHAPTER 4

STRATIGRAPHY

Previous stratigraphic studies were done on the marine deposits that range from Ordovician to Devonian in age and Oligocene-Miocene volcanic deposits (e.g. Dolgoff; 1963; Reso, 1963; Tschanz and Pampeyan, 1970; Ekren et al., 1977; Jayko, 1990; Best et al., 1993; Byron 1995; Jayko, 2007; Best et al. 2013a, b). The marine units include the Ordovician Pogonip Group and Eureka Quartzite, and Devonian Sevy and Simonson dolomites (Figs. 7A & B). In addition, an unknown carbonate unit crops out within the map area; this unit is highly sheared and brecciated, but most likely is Devonian and (or) Silurian in age (e.g., Jayko, 2007). Tertiary-Cretaceous sediments also crop out within the mapped area and regionally predate the Oligocene volcanic rocks (Tschanz and Pampeyan, 1970; Jayko, 2007). The Tertiary-Cretaceous sediments are in fault contact with the Tertiary volcanic rocks in the mapped area. The sequence of the volcanic deposits from older to younger includes Monotony Tuff, Shingle Pass Tuff, Leach Canyon Formation, Pahranagat Formation, Harmony Hill Tuff, and Hiko Tuff. The approximately 14 Ma Kane Wash Tuff (Jayko, 1990, 2007) also is observed within the Paharanagat shear zone, but it does not appear within the mapped area.

PRE-VOLCANIC STRATIGRAPHY

PALEOZOIC ORDOVICIAN AND DEVONIAN UNITS

Two units of Ordovician age crop out in the map area: Pogonip Group and Eureka Quartzite. Reso (1963) described the Pogonip Group in detail in the Pahranagat Range. He divided the Pogonip Group into three limestone units: Lower, Middle, and Upper. The Eureka Quartzite is a silica-cemented Quartz sandstone named by Hague (1883).

Three members of the Pogonip Group are recognized within the mapped area. The lower and middle member are mapped as one unit and the upper member is mapped separately (Plate 1). The lower member consists of limestone with abundant chert nodules, and intraformational pebble conglomerate with sandy beds; no fossils were found although Reso (1963) indicated their presence (Fig. 8 A). The lower part of the middle Pogonip consists of dark gray thin bedded limestone with fewer or lack of chert nodules; as well as fossils like gastropods (Fig. 8 B). The upper part of the middle Pogonip consists of a thinly laminated layer of olive gray and brownish gray limestone (argillaceous limestone) (Fig. 9).

The argillaceous limestone of the middle member of the Pogonip (Fig. 9) is used as a marker bed to separate the middle member from the upper member. In this study, the argillaceous limestone was mapped at the top of the middle Pogonip. However, Reso (1963) mapped this argillaceous limestone within the lower part of the upper Pogonip. The upper unit of Pogonip consists of dark gray limestone, broken shells of various fossils, abundant gastropods and bivalves. Also, a relatively a thin strip of the weathered brownish dolomite occurs within the upper part of the upper Pogonip unit below the Eureka Quartzite (Fig. 10).

An undefined carbonate unit within the study area consists of dark gray, medium to fine grained dolomite. This unit consists of dark gray, medium to fine grained dolomite where less deformed. This unit is highly folded in the middle and intensely brecciated where faulted, particularly on the western side where it is in fault contact with Simonson and Sevy formations. No fossils were found, but Jayko (2007) assigned it a Devonian and/or Silurian age. I suggest that this unit could either belong to Ely-Spring dolomite or Laketown Dolomite, according to stratigraphic order around the study area (e.g. Reso, 1963, Tschanz and Pampeyan, 1970).

The Sevy Dolomite consists of yellowish gray phaneritic to aphanitic dolomite with zones of brecciated quartz-rich sandstone and/or quartzite (Fig. 11 A). This quartz-rich sandstone either belongs to the Oxyoke Canyon Formation (Jayko, 2007) or the uppermost part of the Sevy (Reso, 1963; P. 909).

The Simonson Dolomite overlies the Sevy Dolomite and rests above the rich-quartz sandstone mapped as the top of Sevy. The Simonson Dolomite consists of alternating bands of dark and light gray color, coarse to fine-grained dolomite (Fig. 11 B). The top of the Simonson Dolomite is eroded away within the map area, which makes it difficult to calculate the actual thickness from the map.

TERTIARY-CRETACEOUS SEDIMENTS (TKs)

The Tertiary-Cretaceous sediments are described by Tschanz and Pampeyan (1970) as one of three sedimentary deposits within Lincoln County that unconformably overlie Paleozoic formations and are overlain by late Oligocene-Miocene tuffs (Tschanz and Pampeyan, 1970; Jayko, 1990, 2007). This unit includes a thick layer of conglomerate ranging from a meter to tens of meters thick with clasts of various ages of Paleozoic carbonate and quartzite rocks. Also, it includes freshwater limestone. The Tertiary-Cretaceous sediments unconformably overlie the Ordovician Pogonip Group within the mapped area. Also, this unit is in fault contact with the tuffs as young as 26.4 Ma, the Shingle Pass Formation.

OLIGOCENE-MIOCENE VOLCANIC STRATIGRAPHY

The volcanic stratigraphy of Nevada is well described (e.g., Cook, 1965; Best et al. 1993; Best et al., 2013a, b) in terms of thickness, origin, age, and distribution (Fig. 7 A). The map area is located in an area between the Indian Peak–Caliente caldera complex on the east, the central

Nevada caldera complex on the northwest, and the southern Nevada volcanic field on the west. The mapped tuffs originated from the central Nevada and the Indian Peak-caldera complexes. The Monotony Tuff, Shingle Pass Formation, and Paharanagat Formation (Fig. 7 A) originated from the central Nevada caldera complex whereas the Leach Canyon Formation, Harmony Hills Tuff, and Hiko Tuff originated from the Indian Peak–Caliente caldera complex (Best et. al., 2013a, b).

Each of the ash-flow tuffs in the map area are single cooling units except for the Shingle Pass Formation. Best et al. (2013a) divided the Shingle Pass Formation into five units (Sawmill Canyon Tuff Member, Egan Tuff Member, Tikaboo Tuff Member, Hancock Tuff Member, and Coyote Summit Tuff Member. Within the mapped area only three members are distinguished: Lower Shingle Pass Formation is equivalent to the Coyote Summit Tuff Member, Middle Shingle Pass Formation is equivalent to the Tikaboo Tuff Member, and Upper Shingle Pass Formation is equivalent to the Egan Tuff Member. The extent of the Upper and Middle Shingle Pass Formation is consistent with the thickness distribution by Best et. al. (2013a) whereas the Lower Shingle Pass extent and distribution is not consistent, but expands it (Fig. 12).

CHAPTER 5

STRUCTURE AND DATASET

Since Tschanz and Pampeyan's (1970) work that used apparent offset of units to suggest left-lateral strike-slip, little detailed work has been done on the structural geometry of the PSZ including the MLF. Byron (1995) mapped a small part of the eastern MLF at 1:24000 scale, but her map had a limited extent and did not show structural detail on the western portion of the MLF. In this study, I mapped the western portion of the MLF at 1:12000 scale. Within the mapped area, strike-slip, extensional and local contractional structures were documented. A strike-slip duplex was documented in the east-central part of the area that has a combination of strike-slip, normal and reverse faults. The duplex faults dominantly strike ENE. Also, three fault sets striking NW, N-S, and ENE were mapped around the duplex structure (Fig. 13). The mapped area is divided into three domains; domain A is the duplex structure, domain B lies north-northwest of the duplex structure, and domain C lies west-southwest of the duplex structure (Figs. 14 and 15).

DOMAIN A (DUPLEX STRUCTURE)

The duplex structure is located along the MLF in the eastern and central part of the study area (Plate 1 and 2; Figs. 14 and 15A1). The duplex extends beyond the mapped area to the east where it connects the duplex faults to the master fault or the main strand of the MLF. An orthoimage with 1-meter resolution was used to extrapolate the duplex faults and connect them to the main strand of the MLF adjacent to the map area. (Figs. 14 and 15).

The western end of the MLF is mostly covered by Quaternary deposits and the fault surfaces are not commonly preserved. Therefore, other kinematic indicators such as trend of the folds and

spatial and temporal change in strike of compaction foliations were used to identify the type of motion along the fault zone. The presence of the contractional structures in overall extension and significant change in the strike and dip of both bedding and compaction foliation along the western MLF are consistent with the ENE-striking faults having components of both strike and dip slip. Also, Byron (1995) mapped two strands of the MLF farther east; there, the measured slickenlines of the ENE-striking faults show strike-slip, normal-oblique slip, and reverse-oblique slip.

On the north, the duplex is bounded by a sinistral reverse-oblique fault, FB1, which is an ENE-striking fault, dipping about 75^{o} E (Fig. 15A1). This fault mostly deforms younger rocks such as Oligocene-Miocene tuffs.

On the south, the duplex is bounded by a sinstral normal-oblique fault, FB2, that strikes ENE and dips about 55^{o} W (Fig. 15A1). This fault, from the map, appears to accommodate the maximum change of strike of the compaction foliations along strike of the fault (Figs. 15A1, Plate 1). The constructed cross-sections along with the stratigraphic relationships were used to obtain the fault slip type (Fig. 16, Plate 2). In the footwall of the southern duplex bounding fault is a relatively thick sedimentary unit including conglomerate approximately 10 meters thick and freshwater limestone. This unit unconformably overlies Ordovician Pogonip Group and underlies Oligocene-Miocene tuffs.

In general, the duplex structure consists of 11 faults including the bounding faults. Among the 11 faults, only two faults appear to have reverse-slip motion. Reverse faults can coexist with normal faults (e.g., Fossen, 2010; Dubey, 2014) and may accommodate extension, particularly parallel to the tilted beds. I will explain the kinematics of formation of the local contractional structures in the discussion section in Chapter Six.

The duplex faults deformed both Paleozoic marine and Tertiary volcanic rocks, and contain folds associated with the strike-slip deformation. Four minor folds (I, M1, M2, and N) and two major folds were observed within the Paleozoic units (Fig. 15A1). Fold, FDC1 has a plunge and trend of 14^{o}, 340^{o}; an axial plane strike and dip of 339^{o}, 86^{o} E, and a 120^{o} interlimb angle (Fig. 15A2). Fold, FDC2, which is in contact with the northern domain, has a plunge and trend of 20^{o}, 233^{o}, and an axial plane, strike, and dip of 178^{o}, 24^{o} W with a 155^{o} interlimb angle (Fig. 15A2). Also due to erosion and faulting, most of the fold crests are not preserved well. Therefore, most of the folds are distinguished from the bedding measurements.

Four minor folds were mapped approximately in the middle part of the duplex structure (Figs.15A1 and 17A). Minor fold i trends 194^{o} and plunges 7.8^{o}. This fold is located on the northwestern side of fold FDC2. Minor folds m1and m2 are located on the western side of fold FDC1 and both trend west, 272^{o} and 287^{o}, and plunge 36^{o} W and 38^{o} W, respectively. Contrastingly, minor fold n, which is located at the eastern side of fold, FDC1, trends east about 076^{o} and plunges 18^{o} E.

At the southwestern end of the duplex, fold, FDS1 was mapped, and this fold is covered by Quaternary deposits. This fold is mapped from the cross section and the field data such as the attitude of compaction foliations in the units (Figs. 12 and 16 section CC'; Plate 2). The plunge and trend of this fold is 4^{o}, 37^{o}; it has an axial plane, strike and dip of 220^{o}, 53^{o} W with a 124^{o} interlimb angle (Fig. 15A2). Also, three sets of minor folds were observed in the footwall of the southern duplex bounding fault within the Ordovician Pogonip Group. The minor folds trend N-S, E-W, and NW-SE (Figs. 15A1 and 17B).

DOMAIN B

This domain is entirely underlain by volcanic rocks, with ages from 27 to 18 Ma, and Quaternary deposits (Figs. 14 and 15B1, Plate 1). The youngest exposed rocks are as young as approximately 18.5 Ma (Hiko Tuff), but faulted tuffs as young as 14.5 Ma (Kane Wash Tuff) occur along the MLF, particularly adjacent to the northern domain and to the east. Therefore, domain B and the mapped area contain faults as young as 14.5 Ma or younger. However, no Quaternary faults were mapped within this domain.

Domain B is bounded on the south by ENE-striking faults, and it includes three fault sets that strike N-S, NW and ENE (Plate 1; Figs. 14 and 15B1). The N-S striking fault set cuts the NW-striking fault set, and the ENE-striking fault set both cuts and is cut by the N-S striking fault set (Figs. 13 and 15B1). The ENE-striking faults cut rocks as young as Hiko Tuff.

Two main faults compose the ENE-striking fault set in domain B: FN1 and FN4. FN1 is non-planar along strike and FN1 dips 75^{o} W; the cross-section shows 38 m of throw and 7 m of heave (Fig. 16, Plate 2). This fault accommodates a significant change in the strike and dip of the compaction foliations of the hanging wall along the fault strike. In the hanging wall of this fault along strike, the dip magnitude changes from 40^{o} to 12^{o} E (Fig. 15B1; Plate 1). This characteristic of the change of dip of the hanging wall and the presence of a fault tip at the north end of the fault are compatible with a hybrid or rotational fault in which the dip of the hanging wall changes along a fault strike. FN4 dips 70^{o} W shows 75 m of throw and 26 m heave (Figs. 15B1 and 16, Plate 2).

The N-S striking fault set mostly dips 50 to 65^{o} W and the faults are non-planar along strike. Like the ENE-striking faults, the hanging wall strike and dip of compaction foliations changes

along strike of the N-S striking faults. Therefore, it's most likely that the N-S striking fault set may have a combination of strike and dip-slip motion.

In contrast, the NW-striking fault set is relatively planar along strike and does not show significant change in strike and dip of the hanging wall units along the fault strike. Thus, it seems that the NW-striking fault set has a smaller component of strike-slip and may have dominant dip-slip motion. The NW-striking fault set dips about 75^{o} to 80^{o} W (Figs. 14, 15B1 and 16).

Two faults (X and Y) were mapped based on the orthoimage and unpublished map of Taylor (2015, personal communication) (Figs. 13 and 14). I have no conclusive data to suggest whether fault X has a strike-slip component. In contrast, Fault Y as mapped by Taylor (2015, personal communication) north of the mapped area, does have horizontal slickenlines which indicate that fault Y has a component of strike-slip motion.

Five folds were mapped within this domain. Fold E lies among the N-S striking fault, FN5 and an ENE-striking fault adjacent to the northern duplex bounding fault, FB1, and an inferred fault (Fault X). This fold has a plunge and trend of 2^{o}, 349^{o} an axial plane strike and dip of 181^{o}, 11^{o} W, and an interlimb angle of 152^{o} (Fig. 15B2). This fold formed oblique to both faults the ENE-striking fault adjacent to the fault, FB1and sub-parallel to the fault FN5. These spatial and geometric relations may suggest that this fold is either associated with a strike-slip deformation in which folds formed oblique to the extension direction or this fold formed as a drag fold in the hanging wall of fault FN5 (Fig. 15 B1). The other four folds (A, B, C, and D) are formed either as longitudinal (drag) or transverse folds parallel, sub-parallel or perpendicular and oblique to the fault strikes (Plate 1; Figs. 14 and 15B1). In addition, some of the folds may have formed due to volume change between faults at depth. Detailed descriptions of formation of the folds are found in Chapter Six.

DOMAIN C

This domain mainly exposes Paleozoic and Quaternary units but does contain three volcanic units (Plate 1; Figs. 14 and 15C). The Paleozoic units include the Ordovician Pogonip Group and Ordovician Eureka Quartzite. The Quaternary deposits consist of two units: An older bedded Quaternary unit that dips 5 to 15^{o} E or W and the younger Quaternary unit that consists of non-bedded, unlithified poorly sorted sediments. The volcanic units include Shingle Pass Formation, Harmony Hills Tuff and Hiko Tuff.

Domain C contains three fault sets that strike N-S, ENE, and NW. The N-S striking fault set cut rocks as young as Hiko Tuff. One NW-striking fault is mapped within this domain (Figs. 14 and 15 C). This fault, FS3, dips about 80^{o} W and is located in the eastern part of this domain. The calculated net slip for fault FS3 is 9 m of throw and 2 m heave (Fig. 16, Plate 2).

An ENE-striking fault, FS7, was mapped in the western part of this domain within the Ordovician Pogonip Group (Figs. 14 and 15C). This fault dips about 80^{o} E and is cut by N-S striking fault FS5. A horizontal stylolite parallel to the strike of the fault requires that the maximum principal stress was vertical when the stylolite formed (Fig. 18). The rocks dip 10^{o} to 12^{o} E in the footwall while the dip in the hanging wall is 6^{o} to 8^{o} W. Such data suggest a slightly concave down (anti-listric) fault if it is a normal fault.

MEAN DIRECTION OF STRIKE OF COMPACTION FOLIATIONS

Oligocene-Miocene volcanic units north of the duplex in domain B are divided into three parts; east, central, and west (Fig. 19). Compaction foliations were measured in all of the units: Shingle Pass Formation, Harmony Hills Tuff, and Hiko Tuff. Rose diagrams of strikes of compaction foliations were constructed for individual units according to their distance along the MLF zone. All three Shingle Pass members were plotted together because of their similarity in

age. The Hiko Tuff from east to west shows a mean strike of compaction foliations of 275^{o} ± 13^{o}, 348^{o} ± 13^{o}, and 307^{o} ± 18^{o} in each of the three parts of this domain respectively (Fig. 19). The Harmony Hills Tuff from east to west shows a mean strike of compaction foliations 280 ^{o} ± 18^{o}, 352^{o} ± 11^{o}, and 331^{o} ± 8^{o}, respectively. The Shingle Pass Formation from east to west has a mean strike of compaction foliations of 327^{o} ± 8^{o}, 360^{o} ± 16^{o}, and 341^{o} ± 10^{o}, respectively (Fig. 19). All of these values correspond well with one of the three different mapped fault strikes in this domain.

The constructed rose diagrams show two types of relations; temporal and spatial relationships (Table 4, Fig. 19). Temporally, all compaction foliations strike change anticlockwise consistently in between approximately 26 Ma and 18.5 Ma for all locations; east, center and west. In addition, spatially, a very strong relationship was noticed between mean vector of strike of compaction foliations within the center and west regions (NNW) which distinguishes them from those in the east that have more westerly mean vector of strike of compaction foliations, closer to the duplex structure.

CHAPTER 6

DISCUSSION

FOLDS AND REVERSE FAULTS

Contractional features such as folds and reverse faults are expected within the compressional tectonic regime; however, folds and reverse faults can exist within extensional regions, which are associated with normal and strike-slip faults (Becker, 1995; Schlishe, 1995; Graseman et al., 2005; Fossen, 2010; Dubey, 2014). The spatial distribution, arrangement, and attitude of the folds are of interest of this study to test the kinematic compatibility of structures in the studied area. Hence, I briefly point to the types and origin of folding within extensional regions. Folds in extensional regions can form in different ways and can be explained in different ways such as drag folds (Fig. 20A) including normal and reverse drag (Fig. 21), fault-propagation fold associated with normal and strike-slip faults, folds that accommodate changes in volume with depth (Fig. 22) and en echelon folds associated with strike-slip deformation. Drag folds have various interpretations through time. Some authors used the term drag folds as one type of fault-related fold (Sylverster, 1988; Becker, 1995; Schlische, 1995). In this study, I follow Schlische (1995) and divide the fault-related folds into longitudinal (drag) and transverse folds. A fold is longitudinal or drag (normal and reverse drag) if the fold hingeline forms parallel or sub-parallel to the strike of the fault (Fig. 20A) and a fold is transverse if the fold hingeline forms perpendicular to the fault strike (Fig. 20B) (Schlische, 1995). Hamblin (1965) discussed the formation of reverse drag relative to listric normal faults; In contrast, other authors (King et al., 1988; Gibson et al., 1989; Ma and Kusznir, 1993; Reches and Eidelman, 1995; Schlische, 1995; Grasemann et al., 2003; Graseman et al., 2005) argued that a listric normal fault is not a prerequisite to forming a reverse drag fold. In the case of normal drag, the anticline forms in the

footwall and the syncline forms in the hanging wall (Fig.21A). In contrast, with reverse drag, the anticline forms in the hanging wall and the syncline forms in the footwall (Fig. 21B). Grasemann et al. (2005) associated the formation of normal and reverse drag folds with the dip angle of the faults whereas Schlische (1995) explains that reverse drag forms when displacement decreases with distance from the fault surface. The Grasemann et al. (2005) model showed that in the case of a steeper normal fault a normal drag fold is likely to form; in contrast, a relatively shallower dip angle can form a reverse drag fold (Fig. 21). Transverse folds form as a result of fault displacement variations along strike (Fig. 20B) (Schlische, 1995).

The mapped area contains en echelon, longitudinal and transverse folds. Folds B and E within domain B may have formed as longitudinal folds parallel or sub-parallel to the N-striking fault set. Fold E is an anticline in the hanging wall of fault FN5 and fold B an anticline on the hanging wall of fault FN7. On the other hand, folds A and C may have formed as transverse folds that formed nearly perpendicular to the ENE and N-striking fault sets, respectively (Figs. 14 and 15). Contrastingly, fold C may have formed among faults with different attitudes to accommodate changes in volume with depth (Fig. 20).

En echelon folds form as a series of overlapping folds parallel to each other and oblique about 45^{o} to the extension direction. Examples of en echelon fold may be folds FDC1 and FDC2 within domain A (Fig.15A1). However, en echelon fold may appear as drag folds where they rotate along the strike-slip faults (Sylvester, 1988 referenced to Moody, 1973) but the kinematics of en echelon folds is very different from the drag folds (Sylvester, 1988).

Folds can be used to determine direction and sense of slip within fault zones (e.g. Sylvster, 1988; Becker, 1995). An anti-clockwise spatail change in fold axis orientation was documented within domains A and B. The folds within domain B are interpreted to form as fault related folds that

accommodate change in volume with depth or drag folds, and folds within domain A are interpreted to form either as drag fold or as en echelon folds. The anti-clockwise change in fold axes orientation is compatible with the left-lateral motion of the MLF zone, which is consistent with the mapped left-lateral apparent offset.

Reverse faults can coexist with normal faults. The geometry and charactersitics of such reverese faults are described by Fossen (2010) and Dubey (2014). One such situation can occur when earlier faults are tilted by later faults in a progressive deformation (Fig. 23). Faults mostly evolve into more fault segments as either the hanging wall or the footwall collapses. This hanging wall or footwall collapse may cause rotation and tilting of previous faults. Therefore, faults that formed earlier as normal faults may appear as a reverse fault due to more rotation and tilting of the beds and faults through the evolution of the normal fault system with time (e.g., Fossen, 2010; Dubey, 2014).

The duplex along the MLF contains both normal and apparent reverse faults despite the fact that the duplex lies in a transtentional bend. Two of the reverse faults were mapped within the duplex adjacent to the northern duplex bounding fault (Figs. 15A1 and 23A). Faults inside the duplex are controlled by the bounding faults rather than the regional stress field. Therefore, the bounding faults should form first, and eventually faults inside the duplex start to form. As the duplex grows, it causes rotation and tiliting of the beds and faults inside the duplex (Fig. 23). As a result, faults that formed as an early normal fault may be tilted and appear as a reverse fault in later stages (Fig. 23), which suggests that the apparent reverse faults accommodated extension rather than compression within the duplex.

DEFORMATION STYLE

The kinematics and geometrical relationship between a strike-slip fault zone and the arrangement of faults and folds within it are explained experimentally by the concepts of pure and simple shear deformation (Sylvester, 1988). The mechanism of pure shear deformation was first described by Anderson (1905). Normal faults and extension fractures will form perpendicular to the extension axis, and reverse faults and folds will form perpendicular to shortening axis (Fig. 24). In this case, a conjugate set of complementary sinistral and dextral strike-slip faults may form. It's important to fulfill the requirements of pure-shear deformation that the two conjugate sinistral and dextral strike-slip faults occur simultaneously and have similar amounts of offset (Sylvester, 1988). Therefore, the conjugate faults in pure shear deformation can only accommodate irrotational bulk strain (Sylvester, 1988). A space problem or gap will occur if the two conjugate sets of sinistral and dextral strike-slip faults do not act simultaneously. This gap and space problem can be solved only by rotation and alternating differential slip on each of the conjugate faults.

An alternative model to pure shear deformation is simple shear deformation (Fig. 24). Simple shear is rotational. Thus, it has a monoclinic symmetry of strain and it includes a greater variety of structures than pure shear (Sylvester, 1988). In the case of simple shear, the extensional fractures and normal faults form at an oblique angle to the shortening axis. Also, the folds and reverse faults will form at an oblique angle to the principle deformation zone (i.e., the strike-slip fault) (Fig. 24A). Furthermore, synthetic and antithetic (R and R') Riedel shear fractures form at low and high angle to the principle deformation zone, respectively (Fig. 24).

The PSZ includes three east-northeast-striking parallel or sub-parallel sinistral strike-slip faults that accommodate approximately east-west extension (Tschanz and Pampeyan, 1970; Jayko,

1990; Byron, 1995). To answer the question whether the PSZ experienced simple shear deformation, pure shear deformation or a combination of both is challenging. It's important to understand the geometric relationship, arrangement, and distribution of the extensional and contractional structures within the PSZ and the timing and kinematics of the adjacent structures. In the northern PSZ, near the Arrowhead Mine fault, Evans (2016 MS in progress) documented three fault sets: NW-striking normal faults, NNE-striking normal faults and the ENE-striking sinistral strike-slip Arrowhead Mine fault. In the southern PSZ near the MLF (this study), three fault sets were mapped: NW-striking normal, N-S striking normal, and an ENE-striking oblique and strike-slip fault set, which is the MLF. Contractional features such as folds in the PSZ trend N-S, NW-SE, and SW-NE (this study). Jayko (2007) mapped a few NE-trending folds in the middle part of the PSZ in the vicinity of the Buckhorn fault. Additionally, transtentional strike-slip duplex structures were mapped within the MLF zone and the Arrowhead Mine fault (Evans, 2016 MS in progress; this study) (Figs.13A1 and 23). Approximately, 10^{o}-15^{o} rotation (Axen, 1998; Hudson et al., 1998) and 40^{o}-50^{o} tilting (Hudson et al., 1998; this study) were identified for the western part of the CEZ including the PSZ and MLF zone based on the paleomagnetic data.

The two end member laboratory based and theoretical concepts of simple and pure shear deformation are applied to a homogeneous medium. However, a heterogeneous medium is common in nature. Most people agree that strike-slip deformations occur due to simple shear deformation, but formation of duplexes, bends, or stepovers within strike-slip deformations can generate internal deformation which might cause rock volume change, uplift in the case of a transpressional duplex or subsidence in the case of a transtentional duplex. Therefore, deformation can occur heterogeneously along strike of the strike-slip zones; simple shear

deformation can occur dominantly within less complex strike-slip zones and a combination of pure and simple shear may occur within strike-slip duplexes (Fig. 25).

By comparing the PSZ with the simple and pure shear models, it can be inferred that the PSZ experienced simple shear deformation and/or a combination of simple and pure shear deformation as follows: (1) The absence of a well-defined conjugate set of strike-slip faults with a similar magnitude of offset refutes pure shear deformation. (2) The arrangement of extensional features such as normal faults and contractional features such as folds within the PSZ and MLF area support simple shear deformation. (3) The existence of tilting and rotation documented in the vicinity of the PSZ implies that deformation occurred as a result of simple shear. (4) Contrastingly, the presence and geometries of duplex structures in the northern and southern PSZ along the MLF and Arrowhead Mine fault zones suggest that they may have accommodated a slight rock volume change; thus, a simple shear deformation with a component of pure shear can happen at the vicinity of the duplex structures. The above observations imply that deformation is heterogeneous within the MLF zone; combined simple and pure shear deformation may have occurred dominantly within a restricted region (duplex zone) and simple shear deformation may have occurred across other regions.

TRANSFER ZONES

The heterogeneous distribution of slip on individual normal faults can cause segmentation of extended terranes (Faulds and Varga, 1998). Extended terranes can be partitioned into regionally extensive domains of uniformly and/or oppositely dipping normal fault systems that are associated with tilt-block domains (Stewart, 1980; Faulds and Varga, 1998). The asymmetry of the extended terranes is known from geologic data such as geologic maps, cross-sections, isopach maps and geophysical data such as seismic reflection profiles and gravity data (Faulds

and Varga, 1998). In general, all normal faults systems have to terminate along and across strike either as transfer zones or accommodation zones (Faulds and Varga, 1998). Accommodation zones consist of zones of overlapping fault terminations that can separate either uniformly or oppositely dipping normal faults; the fault systems can strike parallel, oblique, or perpendicular to the extension direction. Contrastingly, transfer zones are defined as discrete zones of strike-slip or oblique-slip faulting striking parallel to the direction of extension. Transfer faults accommodate strain transfer between extended domains. In transfer zones, both strike-slip and oblique-slip faults are closely linked kinematically with major normal fault systems. Transfer zones connect spatially different loci of extension along strike that may have variations in both magnitude and sense of motion. In addition, local normal and reverse faults may form in the vicinity of releasing and restraining fault bends (Faulds and Varga, 1998).

Within the mapped area along the MLF and in the northern PSZ along the Arrowhead Mine fault, ~N-striking normal faults terminate at ENE-striking strike-slip and oblique-slip faults that are most likely parallel or sub-parallel to the extension direction (Evans, 2015; this study). Consequently, I suggest that the MLF is a transfer fault and PSZ is a transfer zone spatially connecting different loci of extension.

East and west of the PSZ lie two different extensional domains with different ages, locations, and magnitudes of extension. On the east is the extensional domain, the Mormon Peak-Tule Springs-Castle Cliffs detachments that was active from 18 Ma to ~7 Ma (Axen, 1993; Bidgoli et al., 2015). On the west is pre-volcanic (Oligocene) extension in the vicinity of the Jumbled Hills (Jayko, 1990) and a younger extensional domain along the Sheep Range detachment system that was active since early Miocene (Guth, 1981, 1990; Axen et al., 1993). A less extended region in the Meadow Valley Mountains and the Sheep Range occupies the area between the two extended

regions (Fig. 6). Extension starts earlier west of the PSZ, about middle Oligocene, and was active into the latest Miocene or Pliocene to present; in contrast, extension starts later, probably late Miocene, east-southeast of the PSZ (Jayko, 1990; Axen et al., 1993; Bidgoli et al., 2015). Therefore, the PSZ including the mapped area appears to be a transfer zone that connects two different extensional domains: the domain of the Mormon Peak-Tule Springs-Castle Cliffs detachments on the east and the Sheep Range detachment system on the west (Fig. 6) (Liggett and Ehrenspeck, 1974; Jayko, 1990: Evans, 2015; this study). This interpretation is consistent with previous models that proposed the PSZ formed as a result of east-west differential crustal extension (Ligget and Ehrenspeck, 1974).

TIMING OF DEFORMATION

Cenozoic extension in the western United States took place episodically. The Basin and Range physiographic province within the western US is related to the latest stage of the Cenozoic extensional tectonic evolution, called Basin and Range extension and occurred at < 10 Ma (Zoback et al., 1981). This last stage of the extension is distinguished from the earlier Cenozoic extension based on an angular unconformity, change in structural configurations such as differences in fault strikes and spacing, and chemistry of magmatism such as basaltic magmatism (Zoback et al., 1981; Taylor and Switzer, 2001).

Taylor and Switzer (2001) previously used a change in fault strike as a proxy for the change in regional stress field. Their interpretation from the fault strike was compatible with other studies (Zoback et al., 1981; Best, 1988; Axen, 1993). Fault strike is not a very sensitive indicator of the principal stress directions (Taylor and Switzer, 2001), but given the limited availability of kinematic indicators, fault strike can be used as a second alternative. Fortunately, local and regional studies around the PSZ previously documented a change in regional field stress

particularly, the direction of least principal stress adjacent to the PSZ (Zoback et al., 1981; Best, 1988; Axen, 1993; Hudson et al., 1998; Switzer and Taylor 2001).

Three sets of faults striking NNW, N-S, and ENE were identified within the southwestern part of the PSZ and the mapped area. The regional least principal stress direction was documented to be approximately ENE for most of Miocene (Best, 1988) which is compatible with the NNW-striking normal fault set. The NNW-striking normal fault set is cut by the ENE and N-S striking fault sets, and so, it is the earliest fault set. Additionally, an E-W least principal stress direction documented after 10 Ma (Zoback et al., 1981) is consistent with the N-S-striking normal fault set. The ENE-striking strike-slip fault set cut and is cut by the N-S striking normal fault set, which suggests that they are synchronous. Importantly, rocks as young as 18-15 Ma are cut by the faults. Thus, the timing of strike-slip deformation within the MLF and PSZ initiated in late Miocene or later according to the mapped cross-cutting relationships and regional stress field direction. In addition, geostatistical analysis of compaction foliations that shows different patterns of strike and dip for tuffs <22 Ma relative to tuffs as old as 26.5 Ma (Fig. 19) is consistent with the fault sets and map cross-cutting relationships. Furthermore, the Quaternary fault scarp documented within domain C implies a Quaternary deformation within the MLF zone and the PSZ.

The timing and sequence of deformation within the PSZ including the MLF can be explained according to the data from this study and regional works around the PSZ as follow: 1. Pliocene to Quaternary deformation is shown by the Quaternary fault scarp mapped within the studied area. 2. Mid-Miocene to Pliocene deformation is documented by N-S and ENE-striking fault sets 3. Early middle Miocene deformation is documented by NW-striking normal faults which cut rocks as young 22 Ma and are cut by the N-S and ENE-striking slip fault sets.

CHAPTER 7

CONCLUSIONS

The timing and loci of extension in the Basin and Range sub-provinces are variable and the structural style includes transfer zones and accommodation zones. Some of the crustal adjustments necessitated by these differences occur along the boundary between the NBR and CBR especially strike-slip zones such as the PSZ and CEZ. The PSZ contains three sinistral strike-slip faults including the MLF. Based on the new map data in 35 km^2 of the western portion of the MLF and published regional works; this study constrained the timing of deformation, structural style and kinematic compatibility of the structures in the western MLF zone. The fault geometry, kinematics, and local and regional geologic events within the NBR-CBR sub-province boundary, in particular within the PSZ and MLF suggest the following interpretations.

1. A left-lateral motion is confirmed for the western MLF based on the orientation of the folds and apparent unit offsets within the MLF zone and previous studies of the eastern MLF zone.
2. The current data show that the MLF continues WSW towards the Desert Range through an extensional strike-slip duplex. This duplex suggests heterogeneous deformation occurred along the MLF zone. The MLF deformation is dominated by simple shear.
3. The origin of contractional features such as apparent reverse faults within the extensional duplex structure is explained by progressive development with tilting and rotation of the early formed faults within the duplex. The apparent reverese faults formed as normal faults and were tilted during progressive deformation.
4. The PSZ including the mapped area appears to be a transfer zone that connects two different extensional domains: the domain characterized by the the Mormon Peak, Tule

Springs, and Castle Cliffs detachments on the east and the Sheep Range detachment system on the west. In addition, the fault geometry within the PSZ including the MLF and Arrowhead Mine fault is compatible with a transfer fault model. Therefore, the PSZ demonstrates a SW continuation of the left-lateral motion of CEZ.

5. The current data show that deformation within the PSZ post-dates volcanism, which supports previous studies around the PSZ. In addition, at least three episodes of deformation are documented within the MLF zone:

    A. Pliocene to Quaternary deformation documented by the Quaternary fault scarp exposed within domain C.

    B. Late Miocene to Pliocene deformation is documented from the cross cutting relationship between fault sets in which the N-S and ENE strike fault sets cut the NW strike fault set.

    C. Early middle Miocene deformation is documented by the NW-striking fault set and rose diagrams of strike of compaction foliations.

6. Pliocene-Quaternary deformation along the MLF, shown by a fault scarp in Quaternary deposit is compatible with the Quaternary faults within and around the PSZ and the seismicity of the region. Therefore, the MLF is part of the active tectonic regime.

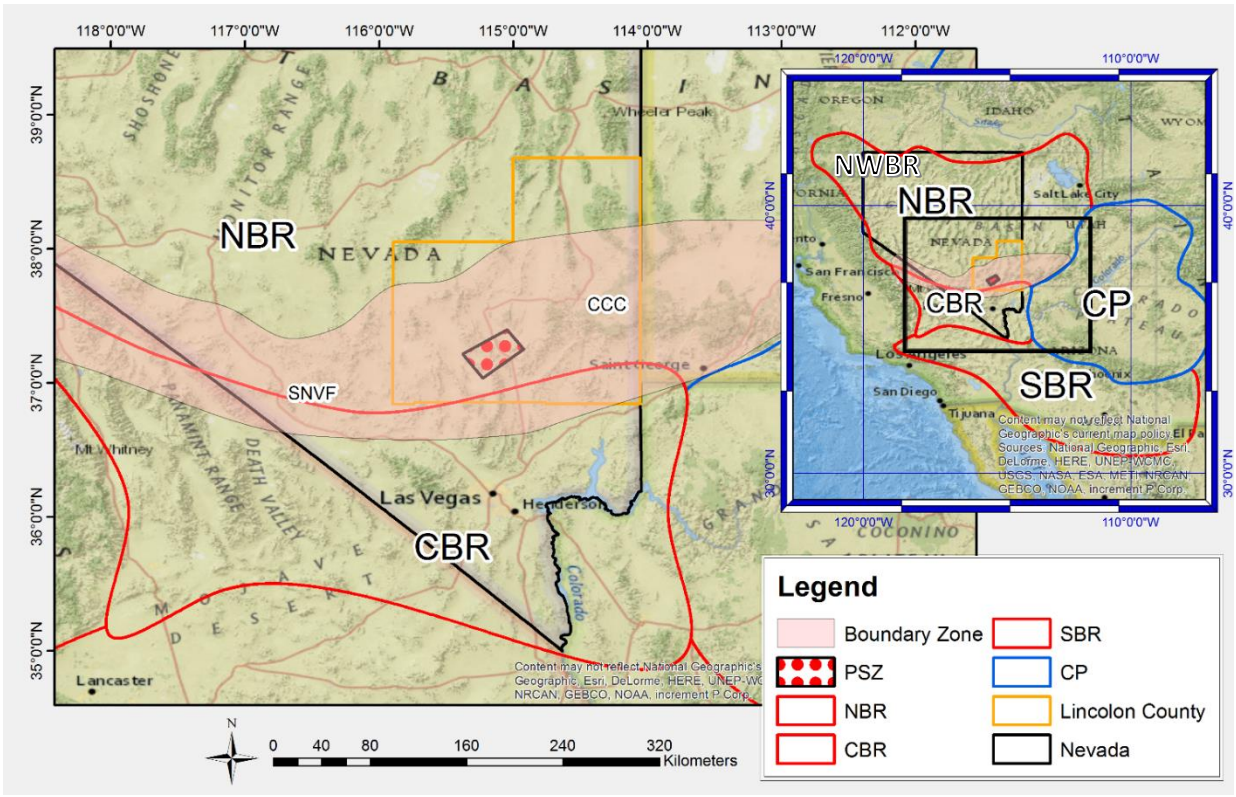

Figure 1. The Pahranagat shear zone and NBR-CBR boundary zone.
The Pahranagat shear zone is located along the boundary zone of the Basin and Range sub-provinces. CBR: Central Basin and Range. NBR: Northern Basin and Range. NWBR: Northwestern Basin and Range SBR: Southern Basin and Range. CCC: Caliente Caldera Complex. SNVF: CP: Colorado Plateau. PSZ: Pahranagat shear zone. Southern Nevada Volcanic Field.

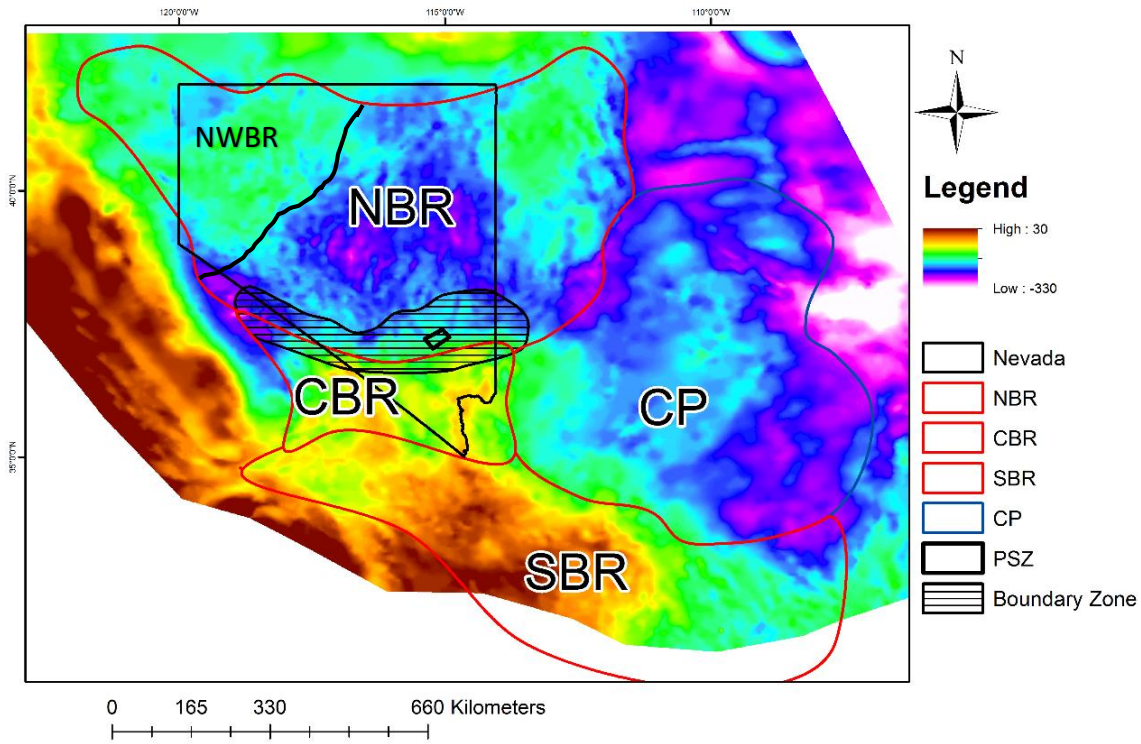

Figure 2. Bouguer gravity map.
The gravity signatures vary among the sub-provinces with a low gravity value in the NBR, a high gravity value in the SBR, and a change of gravity from low to high within the boundary zone between the NBR & CBR. BR: Basin and Range. CBR: Central Basin and Range. NBR: Northern Basin and Range. NWBR: Northwestern Basin and Range SBR: Southern Basin and Range. CP: Colorado Plateau. PSZ: Pahranagat shear zone. Gravity data downloaded from http://gis.utep.edu/subpages/GMData.html.

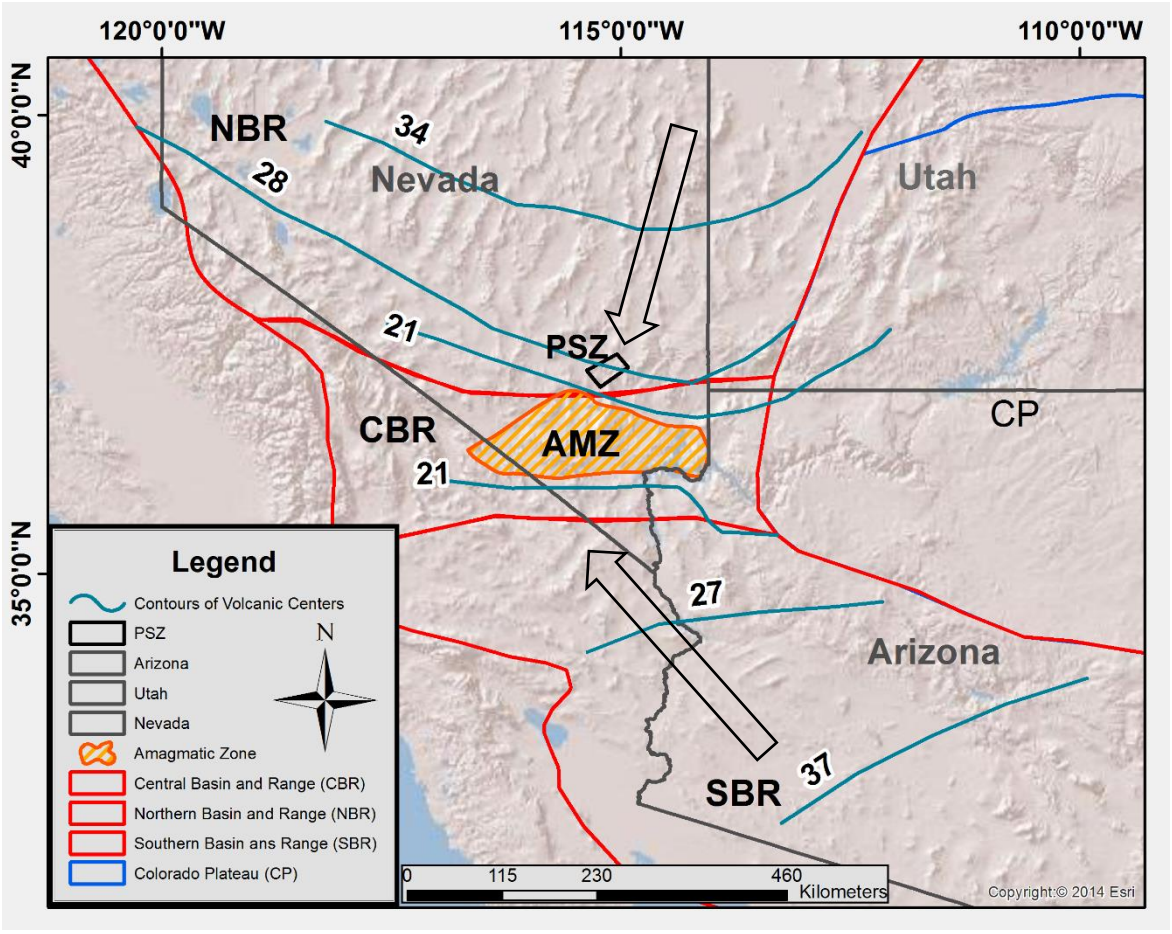

Figure 3. The patterns of magmatism and the amagmatic zone.
Timing of magmatism varies among the Basin and Range sub-provinces; the large arrows show migration of magmatism southward in the Northern Basin and Range (NBR) and northward in Southern Basin and Range (SBR). AMZ shaded region shows amagmatic zone. Contour lines represent isochrons of volcanic centers in Ma after (Rau and Forsyth, 2011). Other abbreviations in Figures 1 and 2.

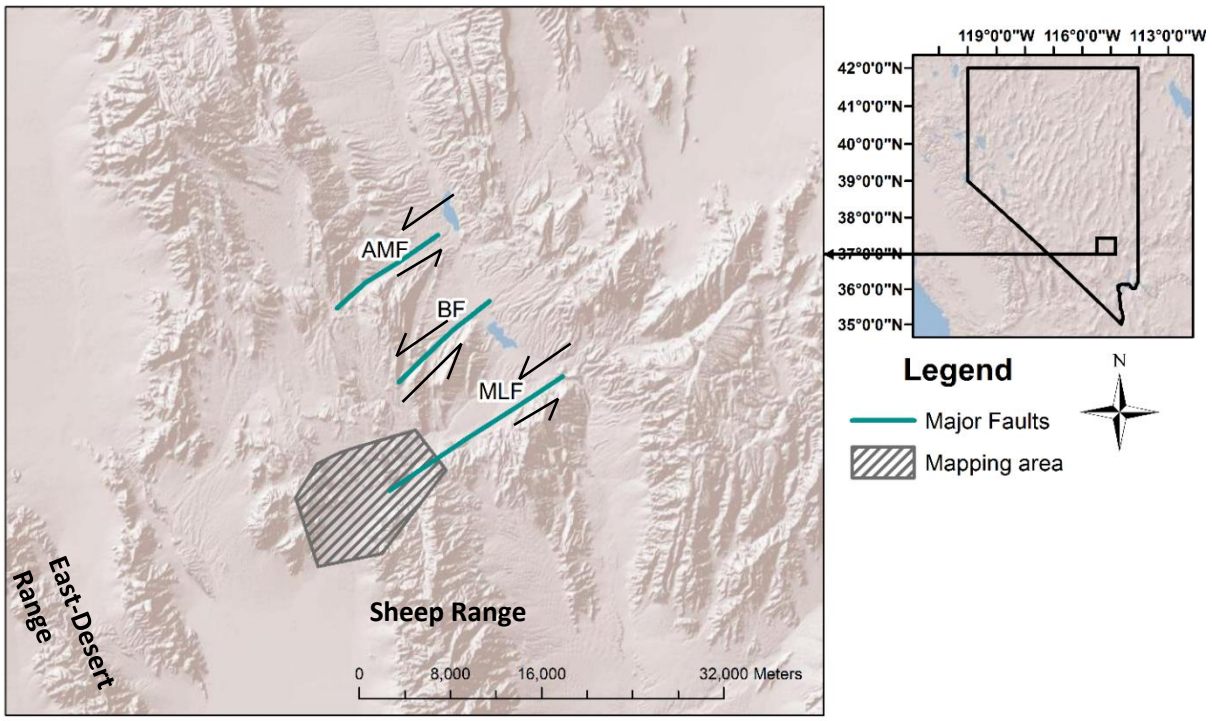

Figure 4. Major faults within the PSZ and location of the mapped area.
Shaded relief map showing the PSZ and major faults in Pahranagat shear zone. Studied area shown by the ruled pattern. AMF: Arrowhead Mine Fault. BF: Buckhorn Fault Zone. MLF: Maynard Lake Fault.

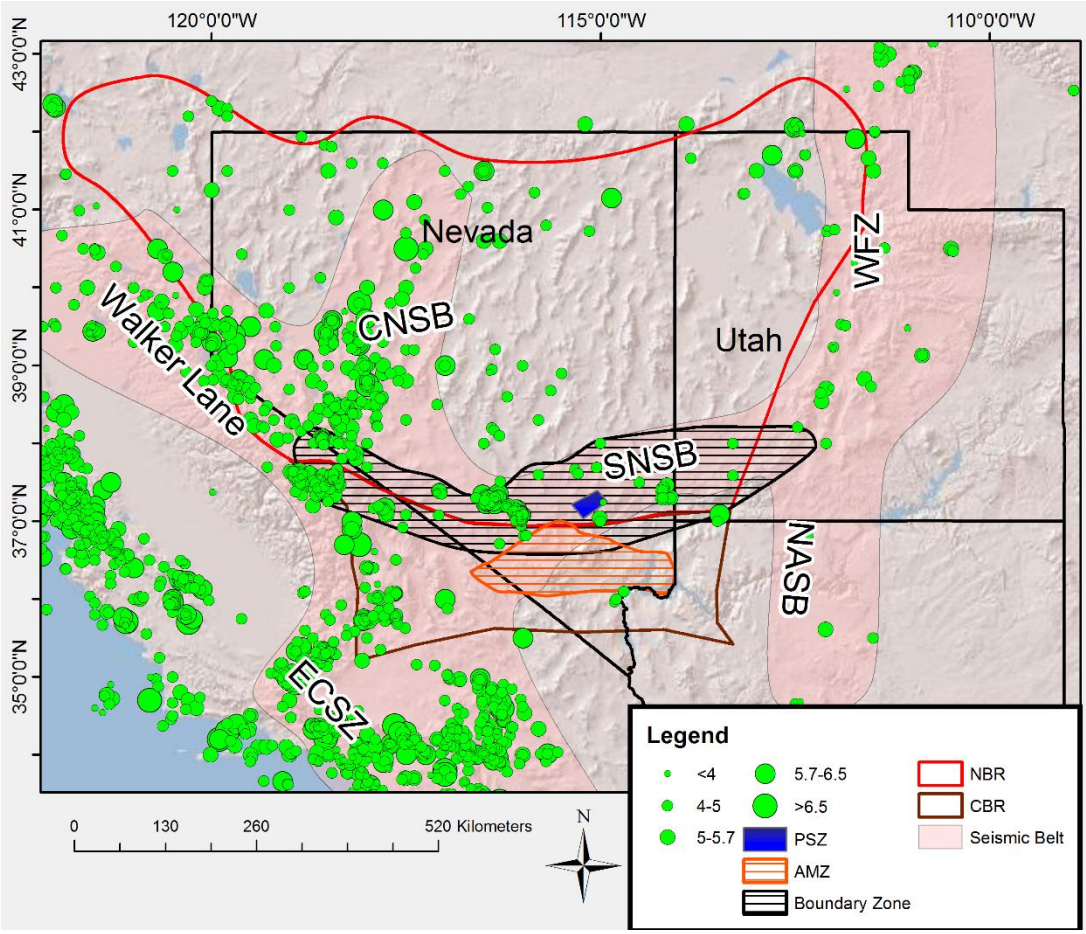

Figure 5. Regions of active seismicity.
Notice that the locations of the amagmatic zone (AMZ), NBR to CBR boundary zone, and Pahranagat Shear Zone (PSZ) coincide with the Southern Nevada Seismic Belt. The size of the green dots represents magnitude of earthquakes. SNSB: Southern Nevada Seismic Belt. WFZ: Wasatch Fault zone. NASB: Northern Arizona Seismic belt. ECSZ: East California Shear Zone. CNSB: Central Nevada Seismic Belt. Earthquake data taken from USGS earthquake database.

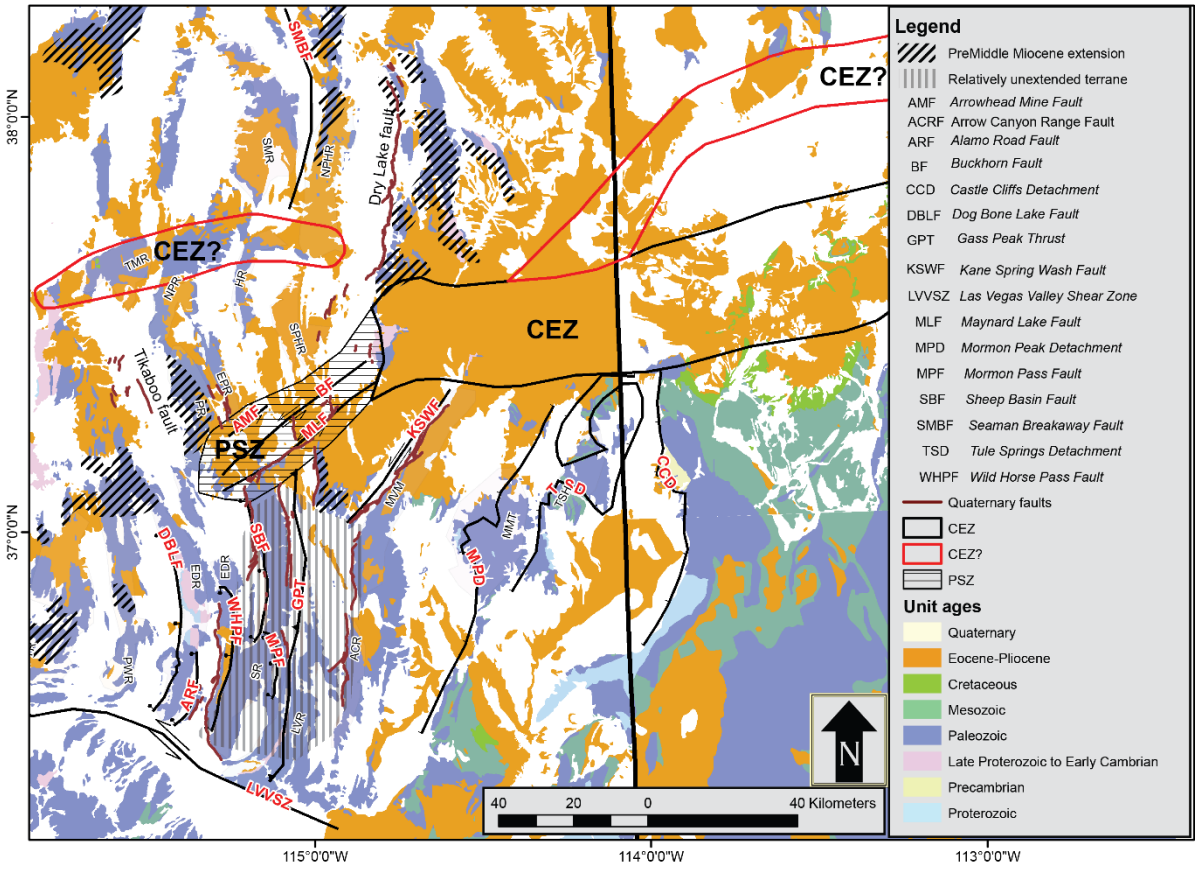

Figure 6. Simplified regional geologic map from the USGS 1:500000 scale (Stewart, 1978).
Shows the Pahranagat shear zone (PSZ) faults and other structures around the PSZ. The location of the structures is taken from (U.S. Geological Survey, Nevada - Nevada Bureau of Mines and Geology, 2006; Guth, 1990; Hudson et al. 1998; Axen, 1998; Petronis et al., 2014; Bidgoli et al., 2015). Approximate age of extension areas taken from Axen et al., (1993). CEZ→Areas of Caliente-Enterprise zone where most previous authors positioned it with; CEZ? →Areas of CEZ where some authors positioned it. TMR: Timpahute Range. SR: Sheep Range, MMT: Mormon Mountain, TSH: Tule Springs Hill, LVR: Las Vegas Range, SPTR: Spotted Range. EDR: East Desert Range, PR: Paharanagat Range, NPR: North Pahranagat Range, EPR: East Pahranagat Range SPHR: South Pahroc Range, NPHR: Northern Pahroc Range, SMR: Seaman Range, PWR: Pintwater Range, DMT: Delamar Mountains.

Age (Ma)	Formation	Thickness	Description
18.6	Hiko Tuff	75 m	Rich in phenocrysts, mapped as one unit. Mostly welded in the study area, however, it includes some less welded lithic tuff in lower elevations. Color varies from grayish red purple to grayish purple. the total phenocryst percentage is ranging between 25 to 30 % for less welded parts and up to 40% for the welded parts. Q: 10-35%, P: 10-35%, S: 15-35%, B: 5-15%
22.2	Harmony Hills Tuff	161 m	Rich in phenocryst, underlies the Hiko tuff. Mapped as one unit, ranges from high welded tuff to poorly welded phenocrysts and realtively large. Also, it has ubiquitous foliated pumice. color varies from very dark grayish red for weathered surface to dark grayish red for fresh surface. The total phenocryst content is 40-60%. Q:0-10%, P: 55-70%, S: 1-3%, B:10-20%, H: 0-15%
22.93	Pahranagat Formation	80 m	A welded to a moderately welded tuff with colors that varies from grayish orange to light reddish brown color. In the studied area the total percentage is in between 20-45%. Q: 21-49%, P:16-42%, S: 22-42%, B: 1-6%
23.8	Leach Canyon Formation	106-153 m	Dark grayish orange to light grayish orange tuff. Total phenocryst percentage is in between 10-30%. Q:20-50%, S:5-40%, P:20-55%, B:0-15%
26.33	Upper Shingle Pass Formation	71 m	
26.77	Middle Shingle Pass Formation	83 m	Distinguished by its trace quartz content. The total phenocryt content is 5-10% total. Q; trace, S:30-40%, P:50-60%, B: 5-15%
26.98	Lower Shingle Pass Formation	86 m	The color is light grayish red to graysih red. Total phenocryst content is 5-15%. Q: 0-5%, S:25-50, P:35-60%, B:5-10%
27.57	Monotony Tuff	45 m	Color is dark grayish red to brown. It is more welded where it appears in higher elevations. Total phenocryst content is 10-20%. Q: 5-15%, S:45-60%, P:25-35%, and B: trace
			The color of the Monotony tuff ranges between grayish orange to very dark grayish orange. Total phenocryst percentage is 10-60%. Q: 5-30%, S:0-15%, P: 45-65%, B: 5-20%, H: 0-10%, Pxc:0-10%

Figure 7 A. Stratigraphic columns of volcanic units.
Thicknesses are measured from the current geologic map were applicable; Ages of volcanic units and modal phenocryst percentage are derived from Best et. al. (1993) and Best et al. (2013a and b).

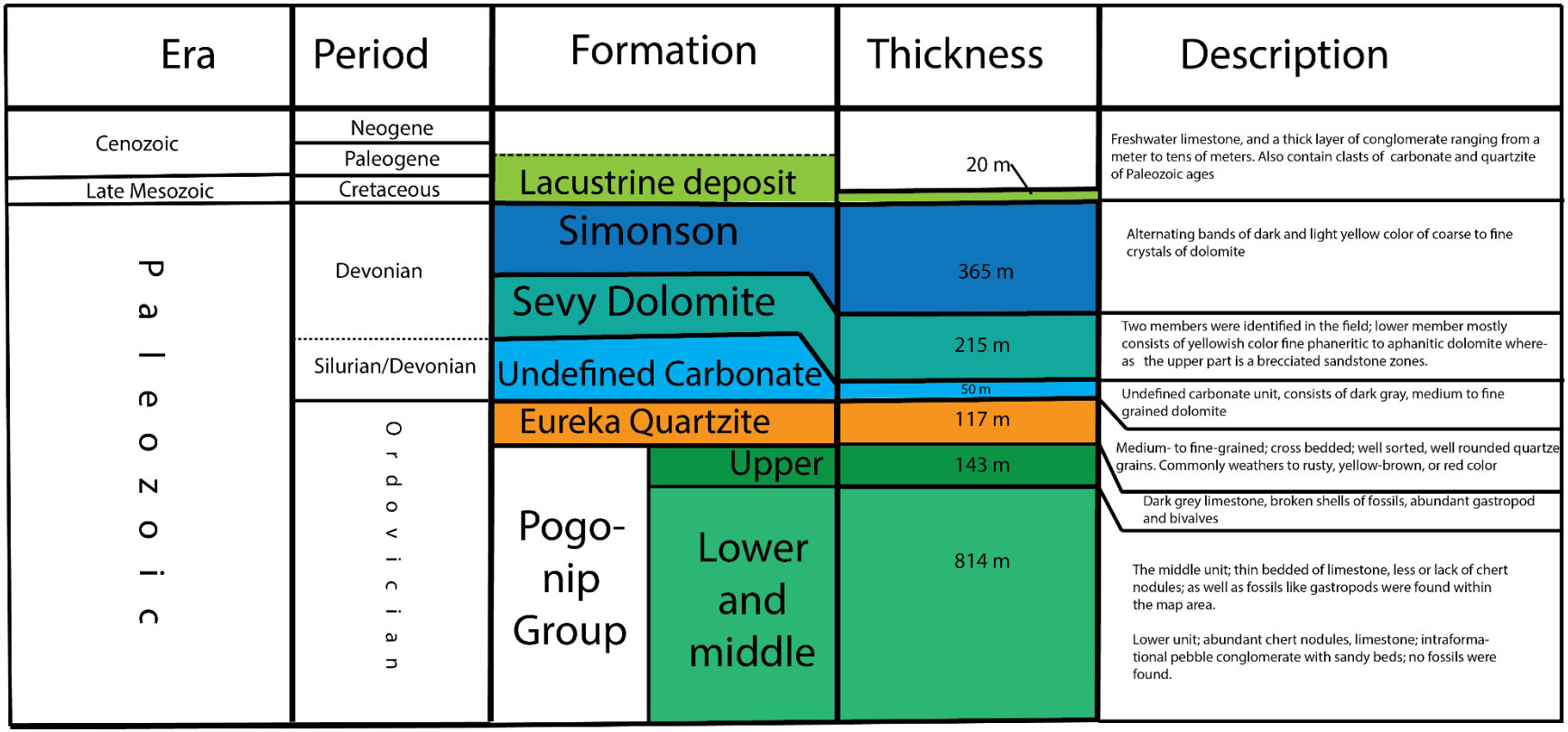

Figure 7 B. Stratigraphic columns of marine and volcanic units.
Stratigraphic column for the volcanic units. B. Stratigraphic column for the pre-volcanic sedimentary units. Thicknesses are measured from the current geologic map were applicable; ages of marine deposits were taken from Reso (1963).

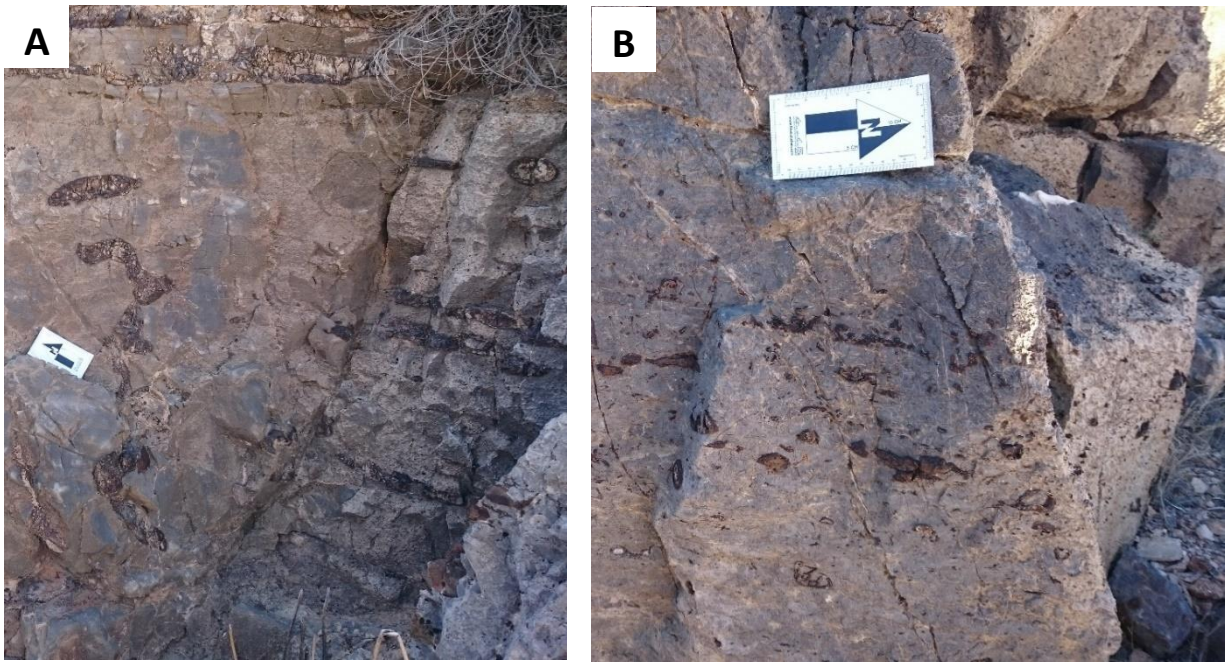

Figure 8. Lithology of Lower and Middle Pogonip Group.
A. lithology of the Lower Pogonip Group. Notice the abundance of chert nodules. B. Shows the lithology of the lower part of the middle member of the Pogonip Group. Notice the abundance of fossils.

Figure 9. Lithology of the Middle Pogonip Group.
Shows the lithology of the upper part of
the middle member of the Pogonip group.

Figure 10. Lithology of the Upper Pogonip Group.
Notice the brownish dolomite strip within the limestone of the Upper member (outlined); the top brownish color is Eureka Quartzite.

A

B

Figure 11. Lithology of Simonson and Sevy dolomites.
A. Dark grey dolomite within the upper part of Simonson Formation. B. Brecciated quartz-rich sandstone and/or quartzite in the upper part of the Sevy Dolomite and base of the Simonson Dolomite.

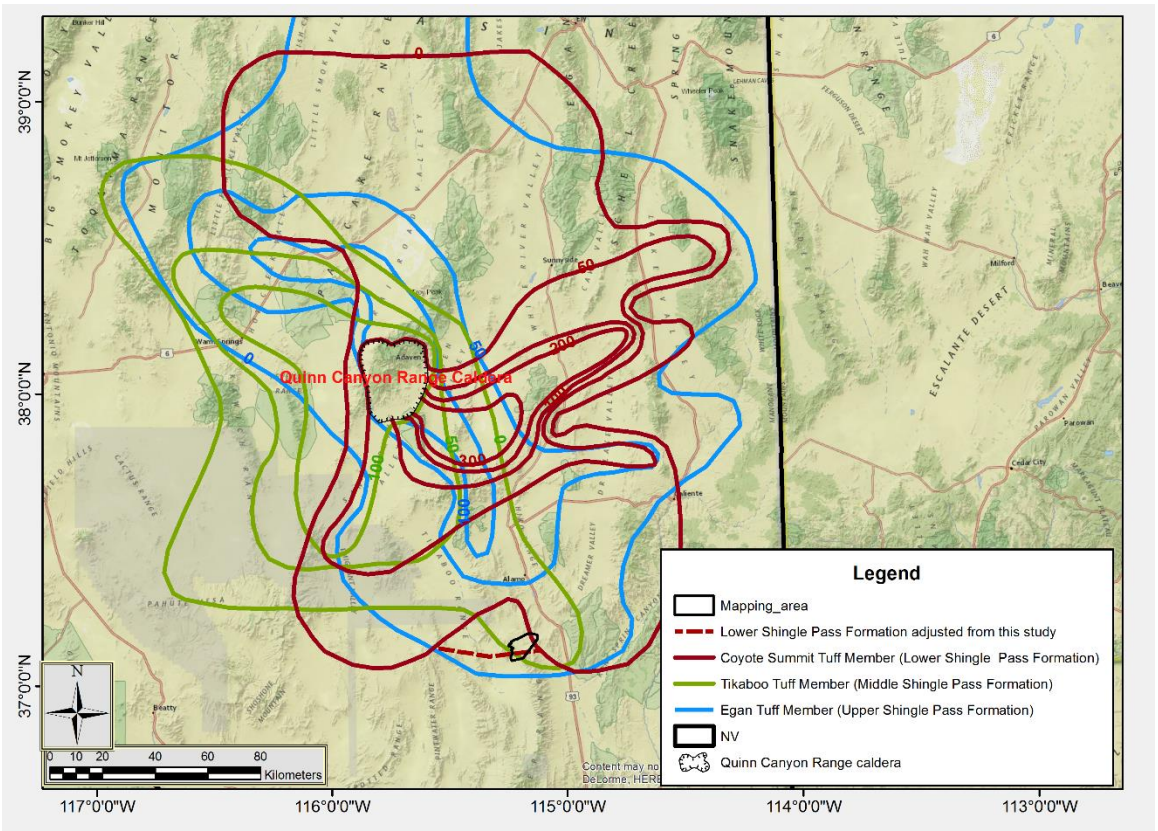

Figure 12. Isopachs of Shingle Pass Formation.
Stratigraphic thicknesses (in meters) and distribution of the Shingle Pass Formation including all three members. Notice the dashed red line shows the adjusted extent of the Lower Shingle Pass Formation (Modified from Best et. al., 2013a).

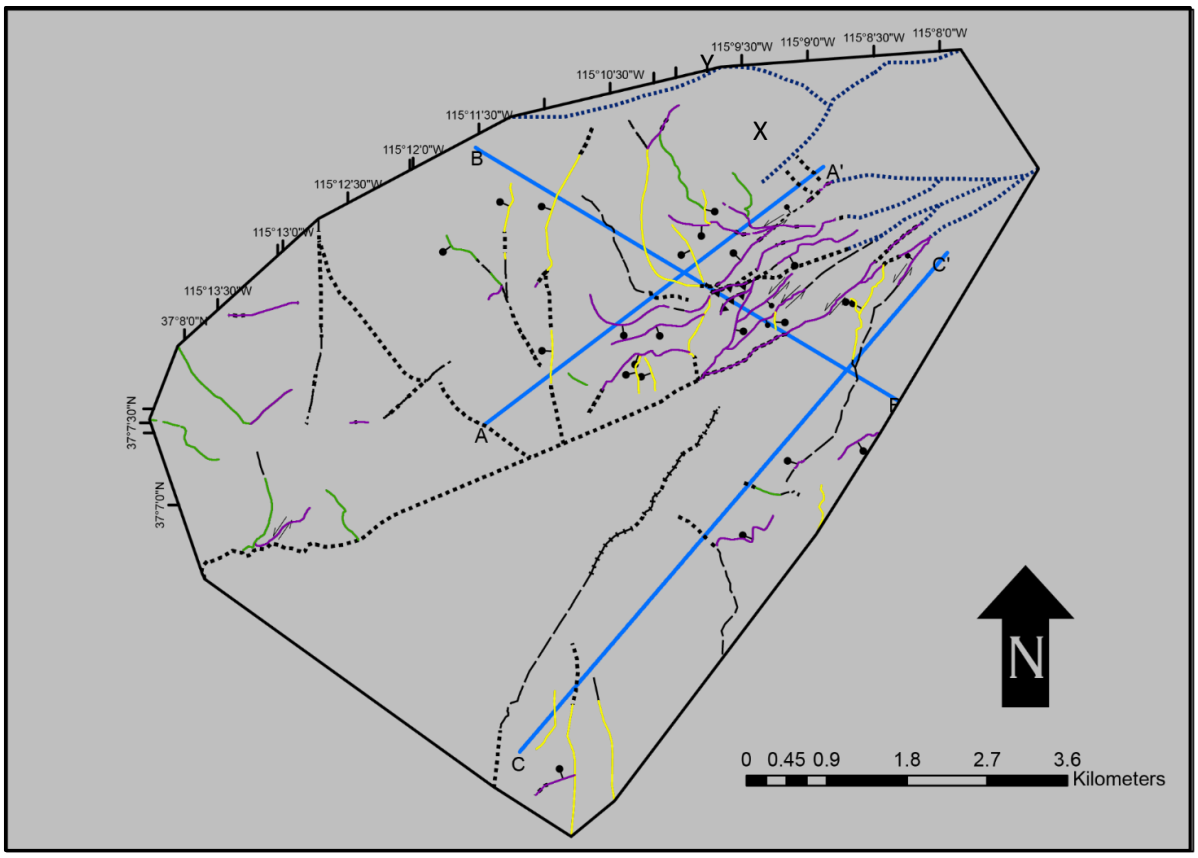

Figure 13. Fault set map.
This figure shows the different strikes of the fault sets mapped. Yellow lines refer to the N-S-striking fault set: Green lines refer to the NW striking fault set: Purple lines refer to the ENE-strike fault set.

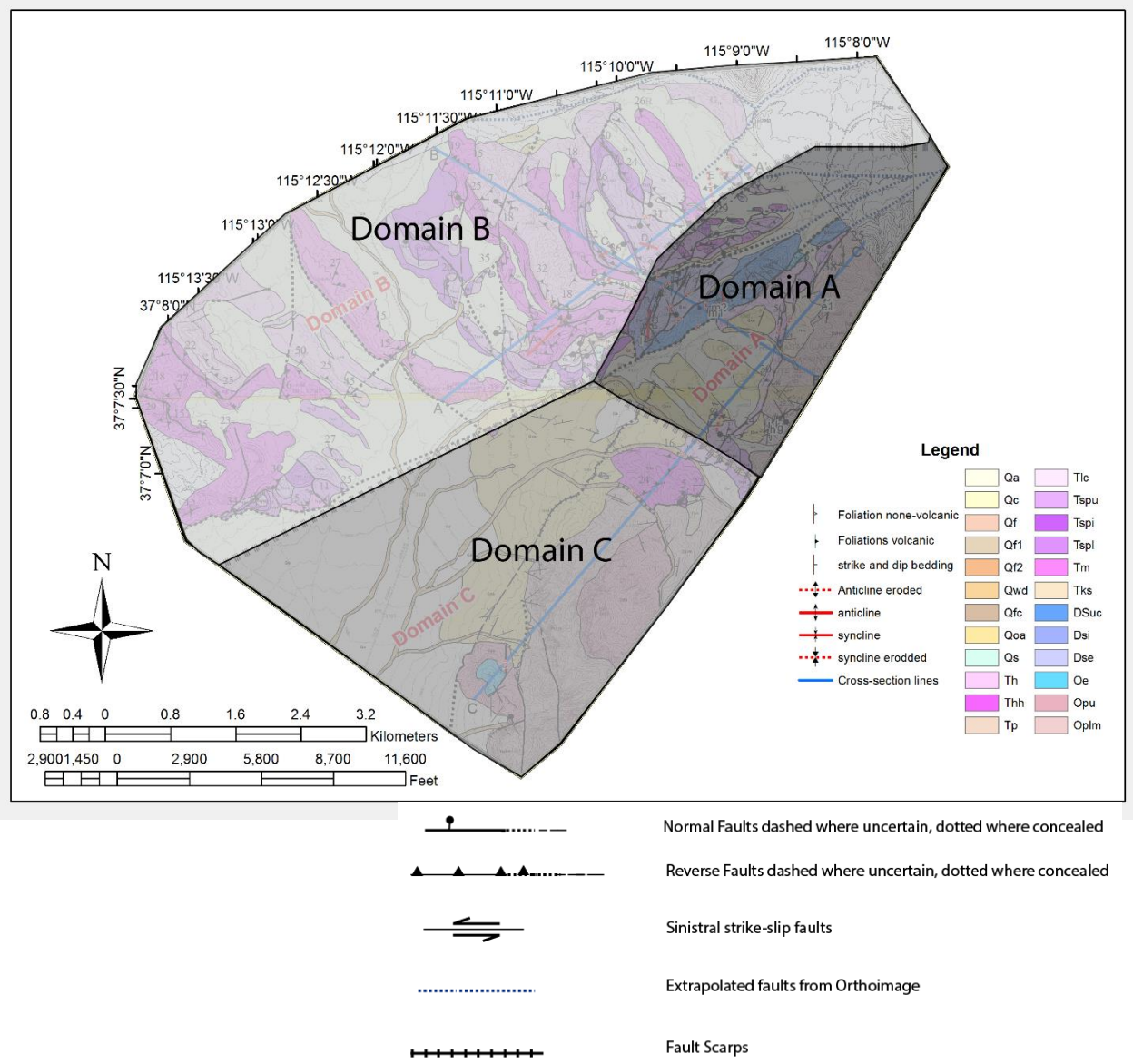

Figure 14. Geologic map of the western Maynard Lake fault.
Index map show locations of domains A, B, and C. For detail description of the units refer to Plate 1 in Appendix 1. The blue dotted lines represent faults that were extrapolated based on 1-meter resolution ortho-imagery. Refer to Plate 1 for the detailed map at 1:12000 scale.

A1

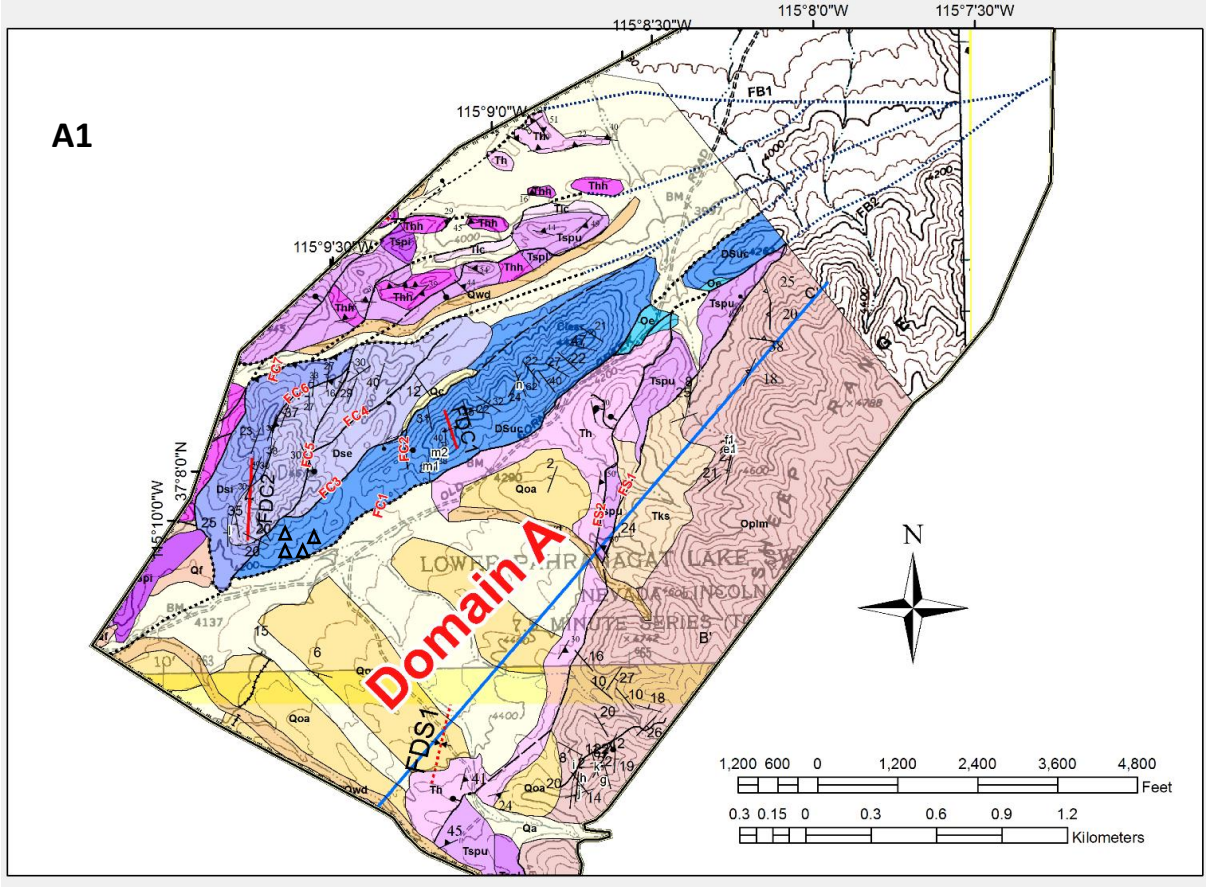
115°8'0"W
115°7'30"W
115°8'30"W
115°9'0"W
115°9'30"W
37°8'0"N
115°10'0"W
FB1
FB2
FDC1
FDC2
FDS1
Domain A
N
1,200 600 0 1,200 2,400 3,600 4,800
Feet
0.3 0.15 0 0.3 0.6 0.9 1.2
Kilometers

A2

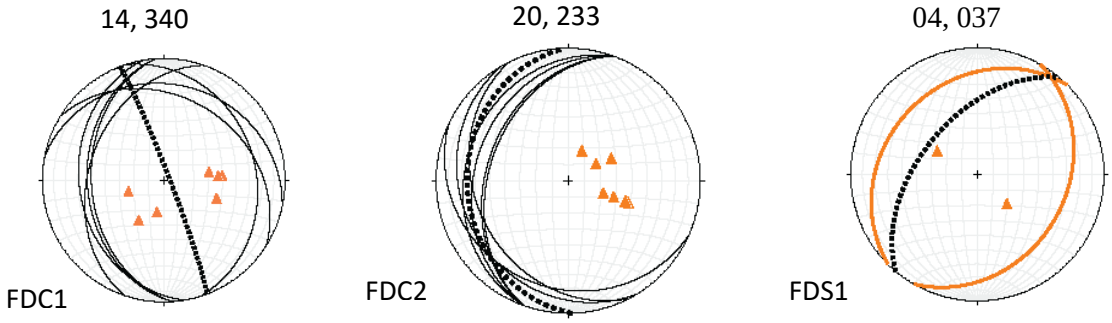
14, 340
FDC1
20, 233
FDC2
04, 037
FDS1

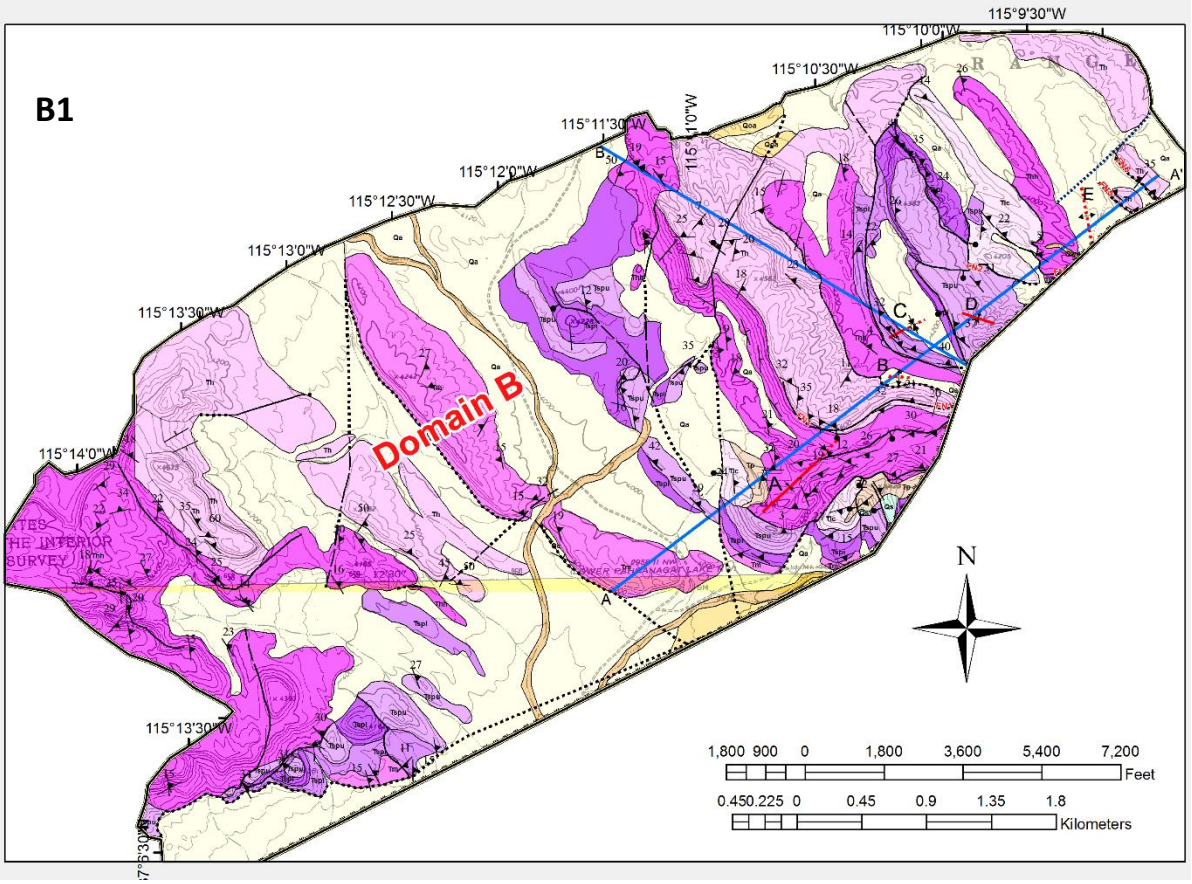
B1
115°9'30"W
115°10'0"W
115°10'30"W
115°11'0"W
115°11'30"W
115°12'0"W
115°12'30"W
115°13'0"W
115°13'30"W
115°14'0"W
Domain B
A
A'
B
C
D
E
N
1,800 900 0 1,800 3,600 5,400 7,200
Feet
0.450.225 0 0.45 0.9 1.35 1.8
Kilometers

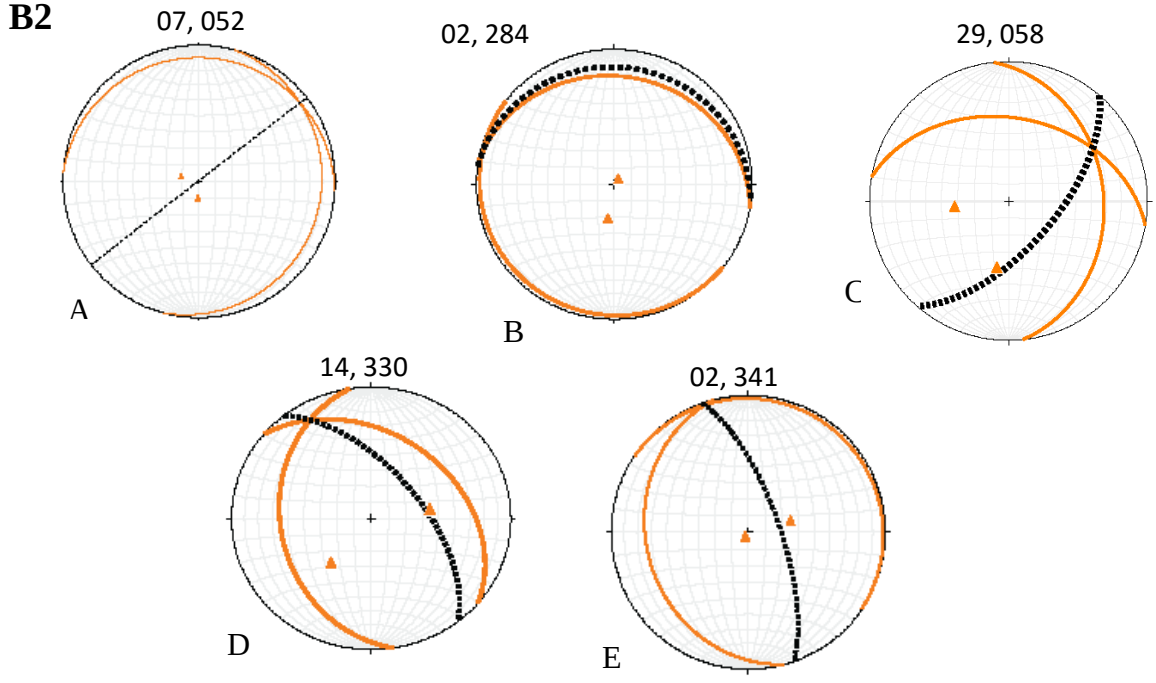
B2
07, 052
A
02, 284
B
29, 058
C
14, 330
D
02, 341
E

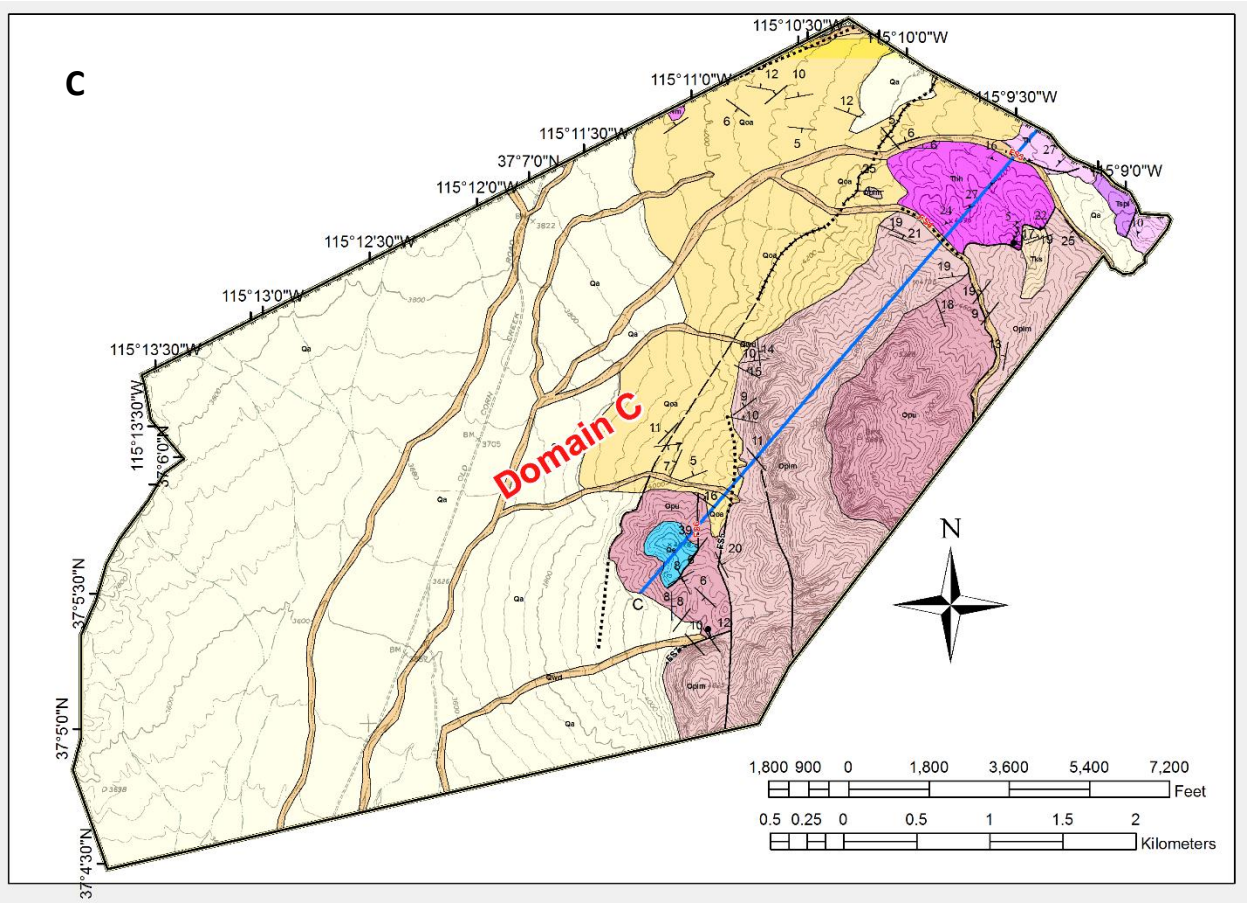

Figure 15. Structural domains and stereographs of folds.
A1. Geologic map showing units and structures of domain A. Triangles indicate intensely brecciated areas. A2. Plotted stereographs of folds: FDC1, FDC2 and FDS1. B1. Geologic map showing units and structures of domain B. B2. Plotted stereograph of folds: A, B, C, D and E.
C. Geologic map shows units and structures of domain C. Refer to Appendix 2 for the fold data.

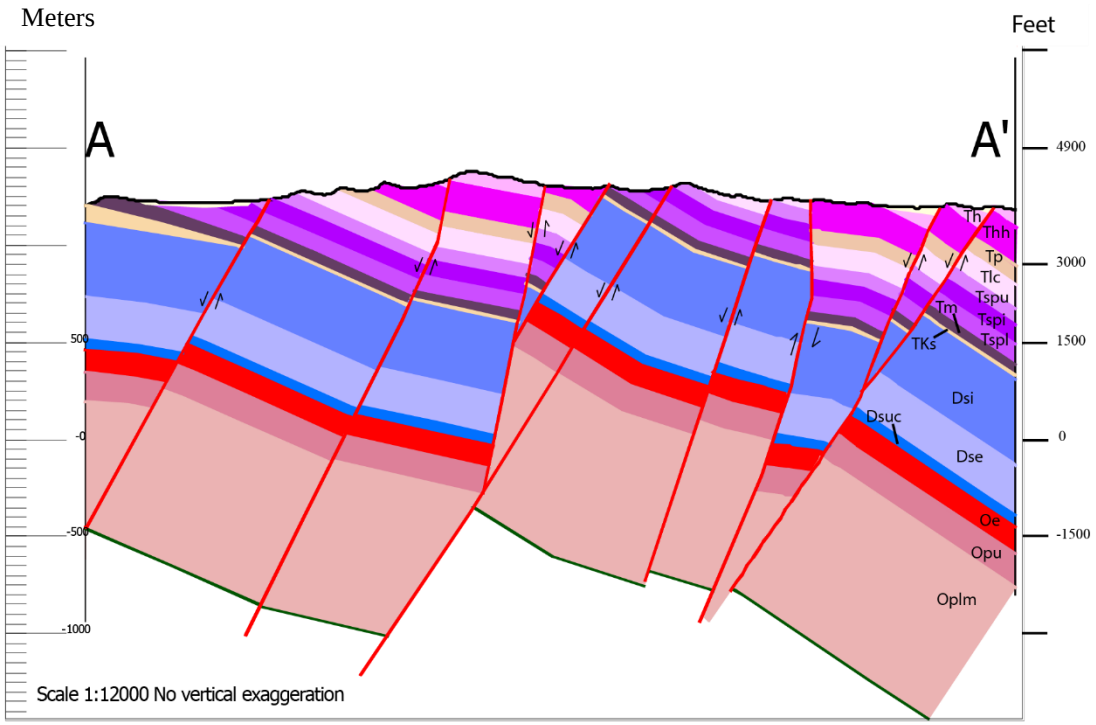
Meters
Feet
A
A'
4900
3000
1500
0
-1500
500
-0
-500
-1000
Th
Thh
Tp
Tlc
Tspu
Tspi
Tspl
Tm
TKs
Dsi
Dsuc
Dse
Oe
Opu
Oplm
Scale 1:12000 No vertical exaggeration

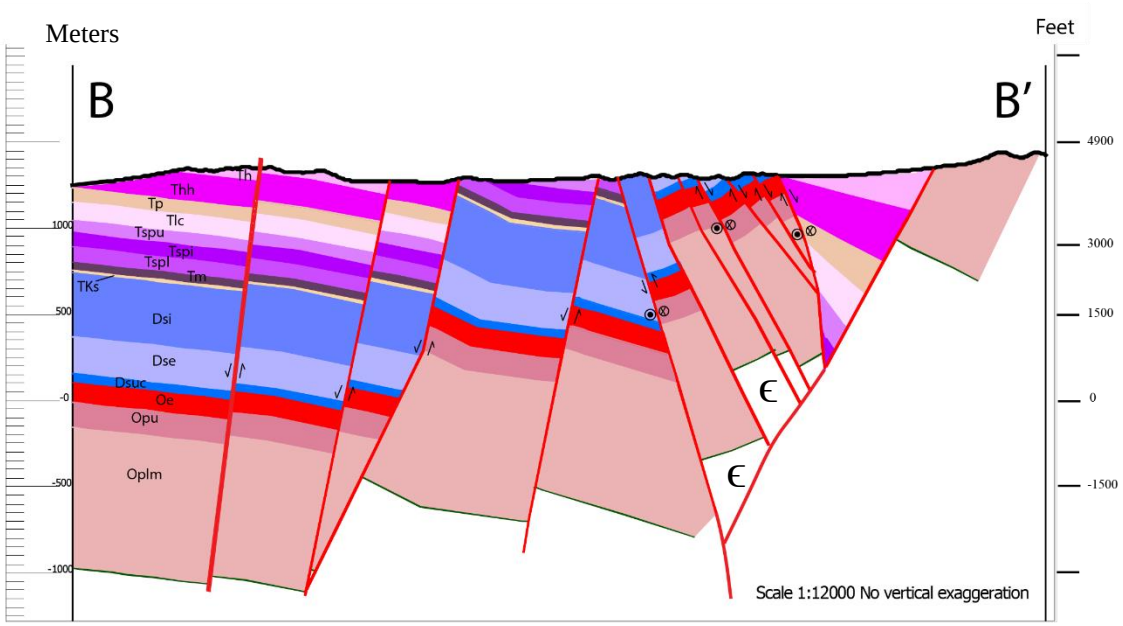
Meters
Feet
B
B'
4900
3000
1500
0
-1500
1000
500
-0
-500
-1000
Th
Thh
Tp
Tlc
Tspu
Tspi
Tspl
Tm
TKs
Dsi
Dse
Dsuc
Oe
Opu
Oplm
Scale 1:12000 No vertical exaggeration

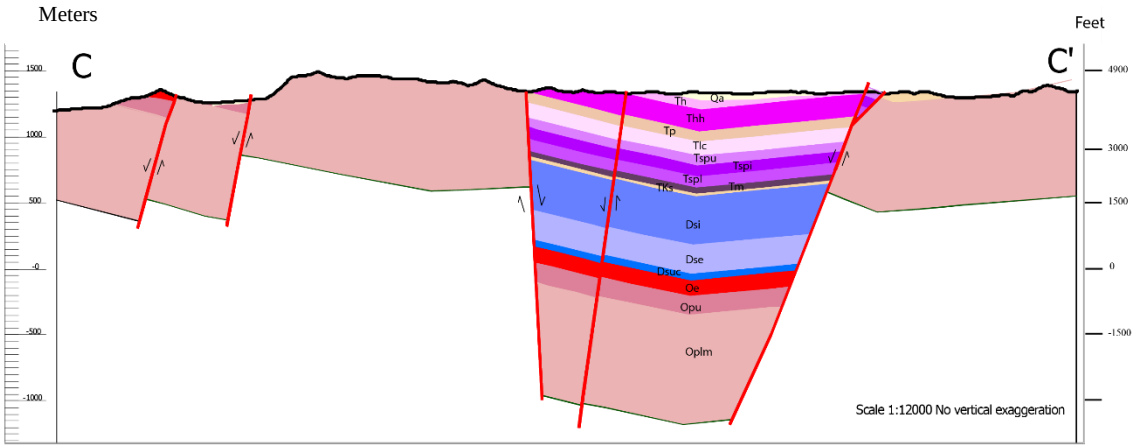

Figure 16. Geologic cross-sections.
Cross-sections AA', BB', and CC'. Locations of the section lines are plotted in figures 13 and 14, and plate 1.

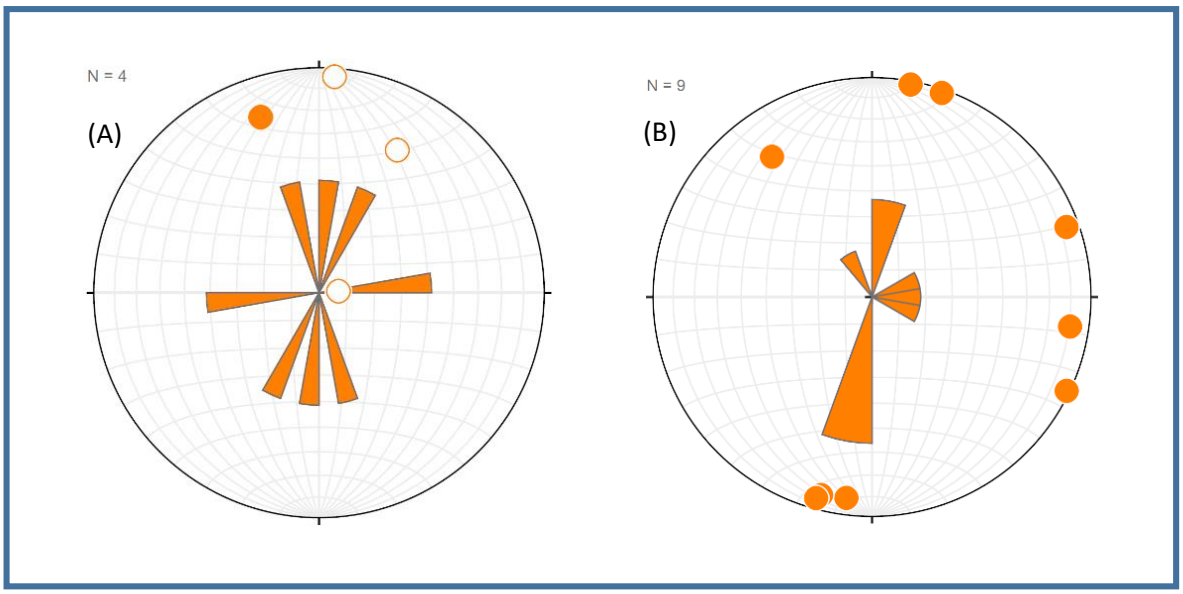

Figure 17. Rose diagrams of the trend of the fold axes of minor folds.
(A). Shows rose diagram of the fold axis trend of minor folds i, m1, m2, and n which are approximately in the middle of the strike-slip duplex. (B). Shows rose diagram of trend of fold axes for the minor folds, i, j, k, h, g, e1, e2, f1, and f2 which are adjacent to the southern boundary of the strike-slip duplex. Notice: clockwise change of the minor fold axis southeast of the strike-slip duplex structure. The locations of the folds are shown on Figure 15A1. Also, the geographic coordination values are given in Table 3.

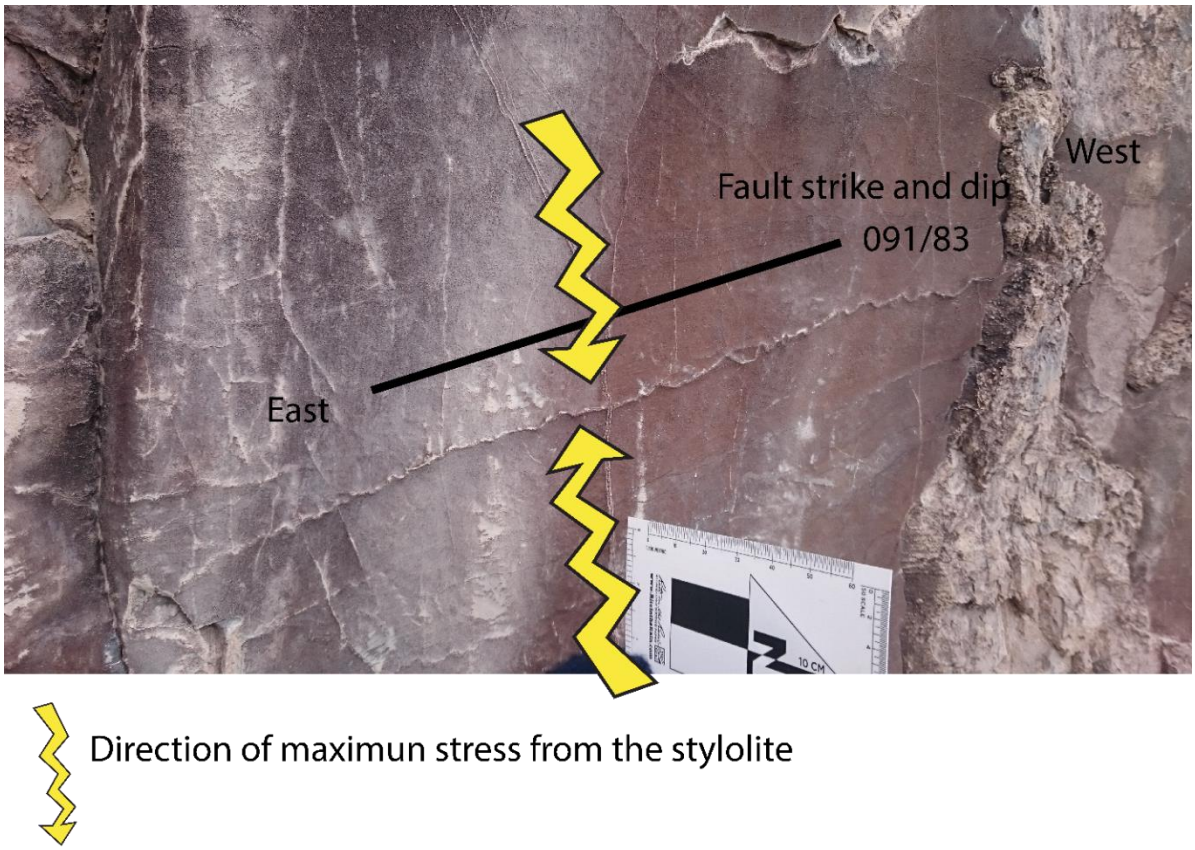

Figure 18. ENE-striking fault surface within domain C.
Notice the formation of the stylolite parallel to the strike of the fault. The maximum principal stress direction is inferred from the formation of the stylolite. Maximum principal stress needs to be vertical to form a horizontal stylolite.

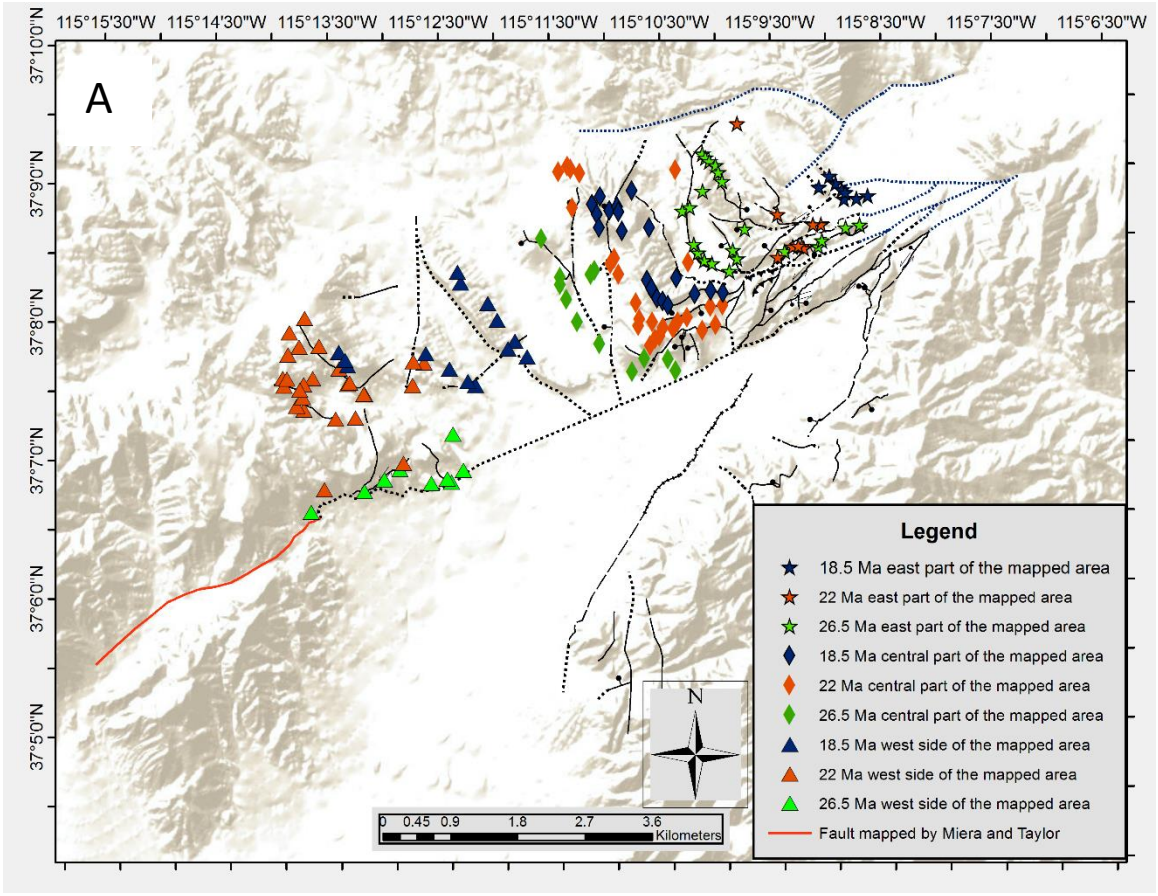

Figure 19. Structural map and spatial distribution of compaction foliation of different ages.
A. Structural map shows faults and locations of compaction foliations that were used to construct rose diagrams. B. Rose diagrams show change in the strike of the compaction foliations from the eastern side of the map area towards western side. Tsp: Shingle Pass Formation, Thh: Harmony Hills Tuff, Th: Hiko Tuff. The y-axis represents age of units, and the x-axis represents distance from the eastern side of the map area towards the western part of the map area. Notice temporally, all compaction foliations strike changes anticlockwise consistently in between approximately 26 Ma to 18.5 Ma for all locations; east, center and west of study area. The stars refer to the eastern map area, diamonds refer to the central central map area, and triangles refer to western map are

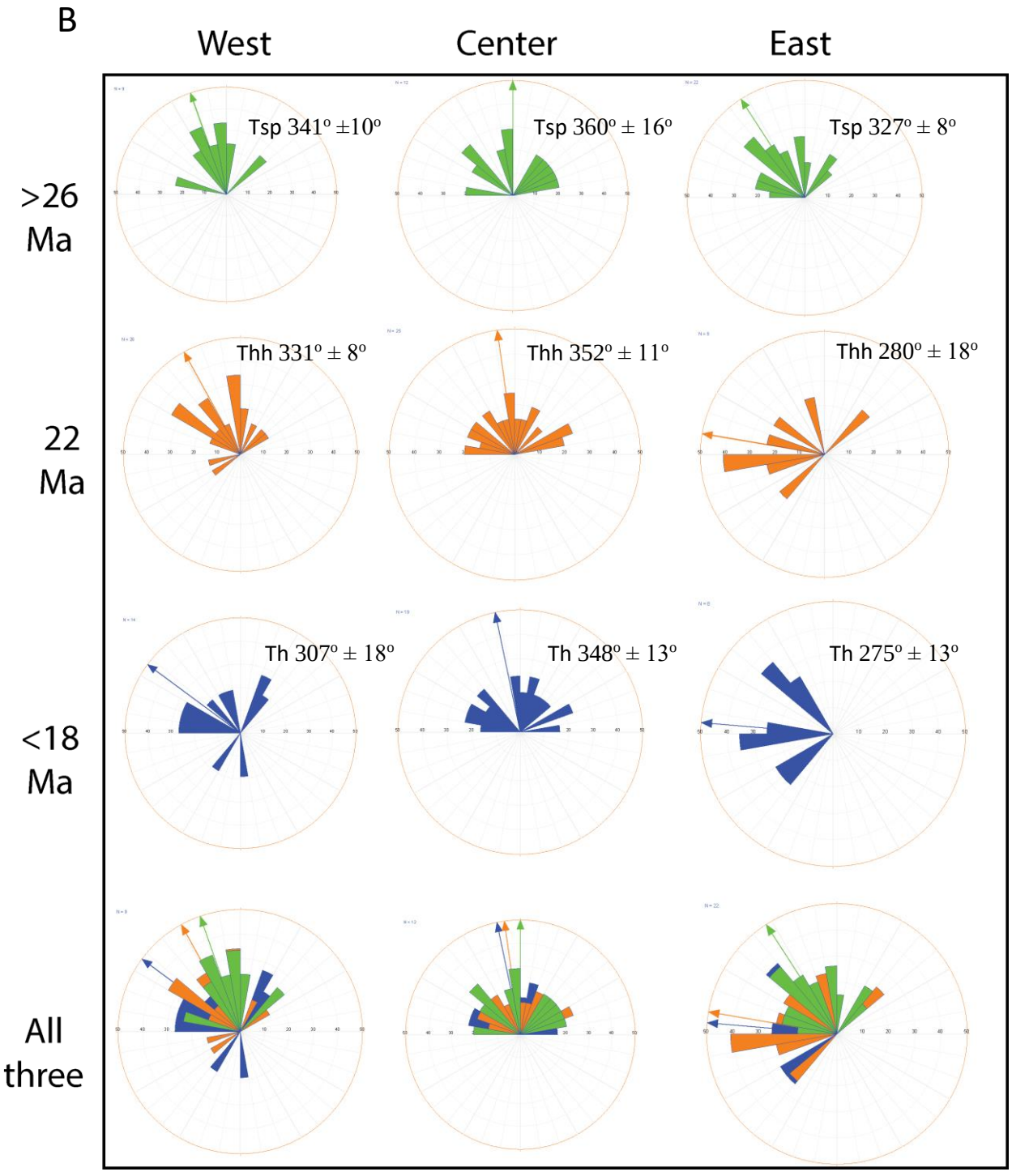
B
West
Center
East
>26 Ma
22 Ma
<18 Ma
All three
Tsp 341° ±10°
Tsp 360° ± 16°
Tsp 327° ± 8°
Thh 331° ± 8°
Thh 352° ± 11°
Thh 280° ± 18°
Th 307° ± 18°
Th 348° ± 13°
Th 275° ± 13°

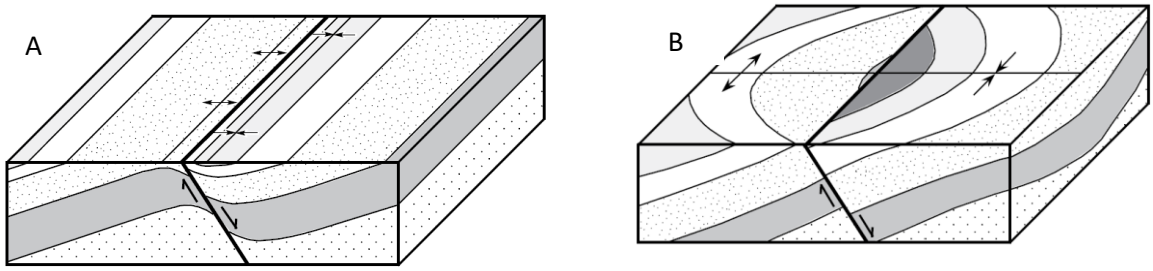

Figure 20. Longitudinal and transverse fold.
A. Shows the formation of a longitudinal drag fold parallel to the fault strike. B. Shows the formation of a transverse drag fold perpendicular to the fault strike (After Schlische, 1995).

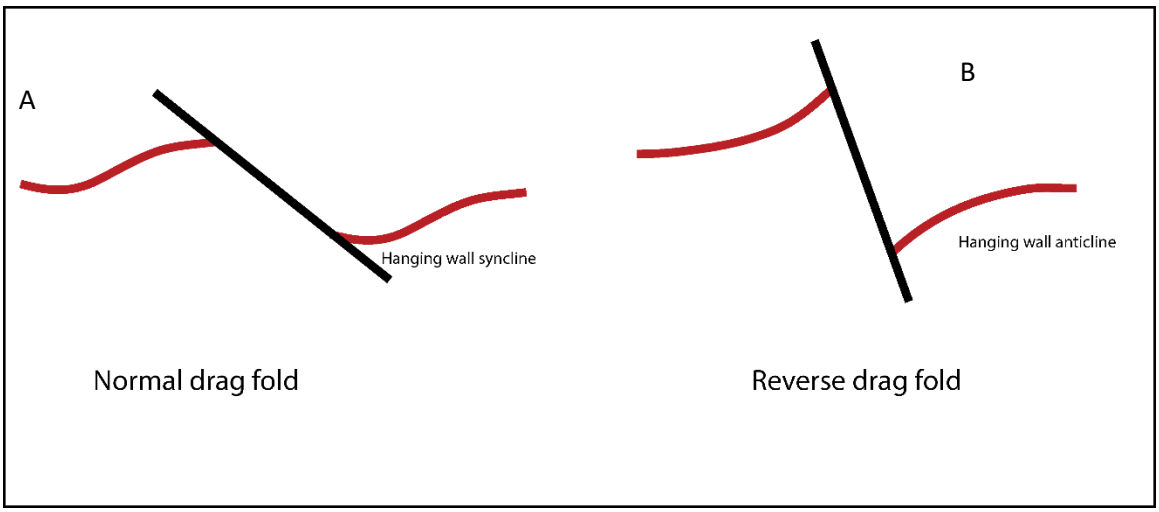

Figure 21. Geometry of longitudinal drag folds.
A. Normal drag fold along a relatively low-angle normal fault. Notice formation of a syncline in the hanging wall and an anticline in the footwall. B. Reverse drag fold along a relatively high angle normal fault. Notice formation of an anticline in the hanging wall and a syncline in the footwall (Modified from Grassman et al., 2005)

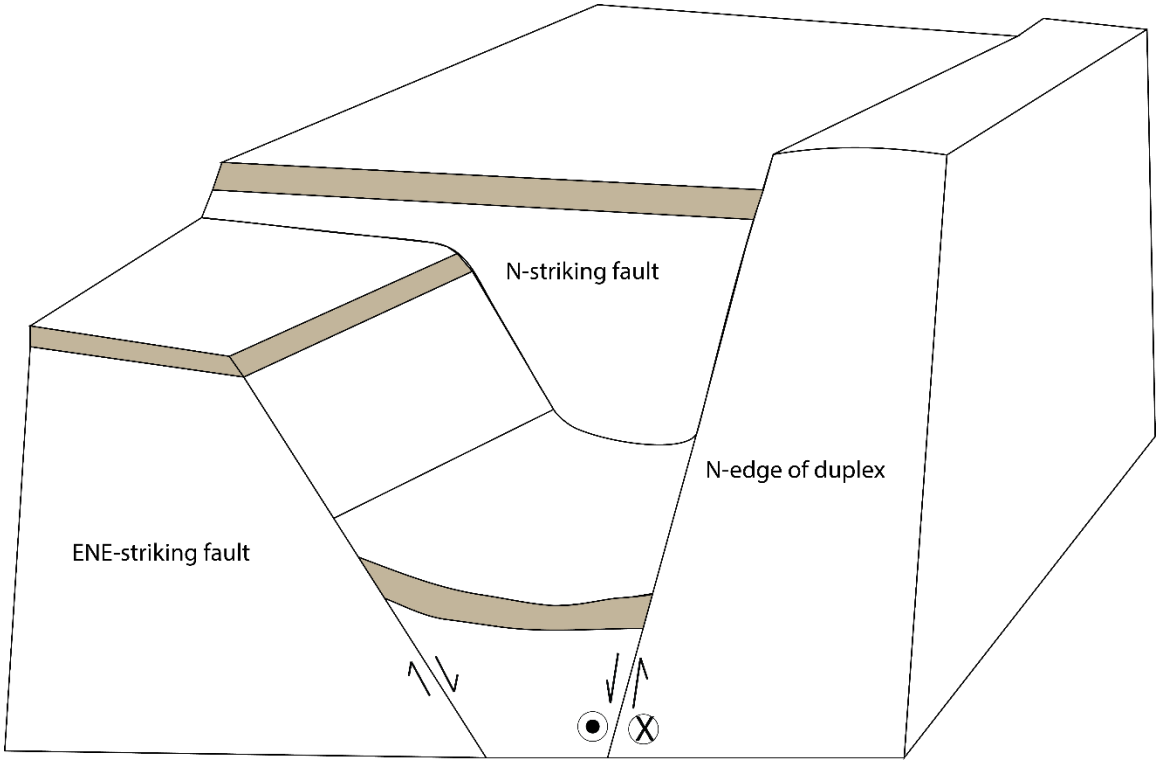

Figure 22. Cartoon model showing a fold formed between fault-sets with different strikes.
The formed drag fold is a transverse fold if it's made by the north-striking fault and the drag fold is a longitudinal fault if it's formed by the ENE-striking fault. The fold may also be a result of a downward decrease in rock volume between the faults, which requires local shortening. Note: Usually longitudinal and transverse drag folds can be distinguished from the cross-section if it's formed by a single and/or uniform fault strike trend, also, they are easily distinguished in the map view.

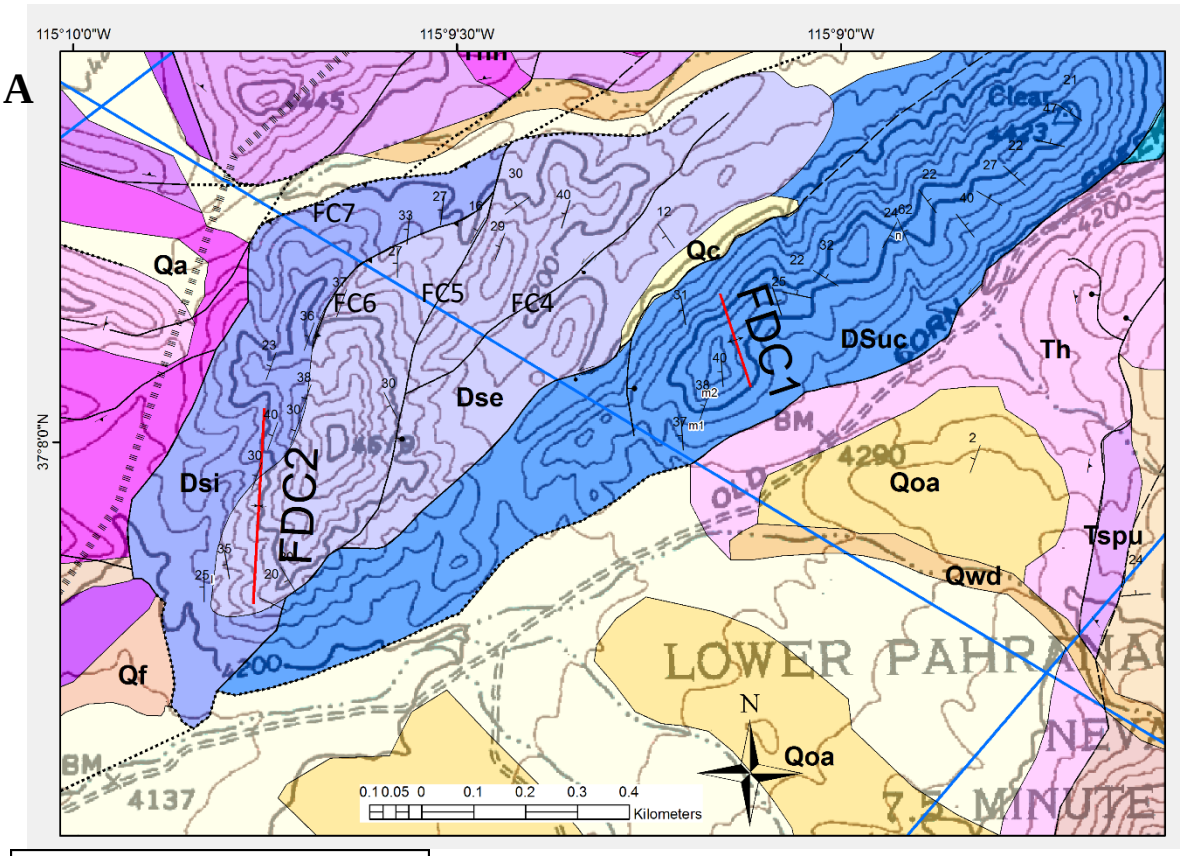

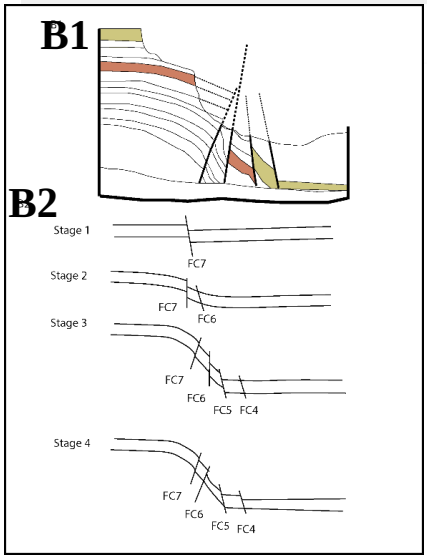

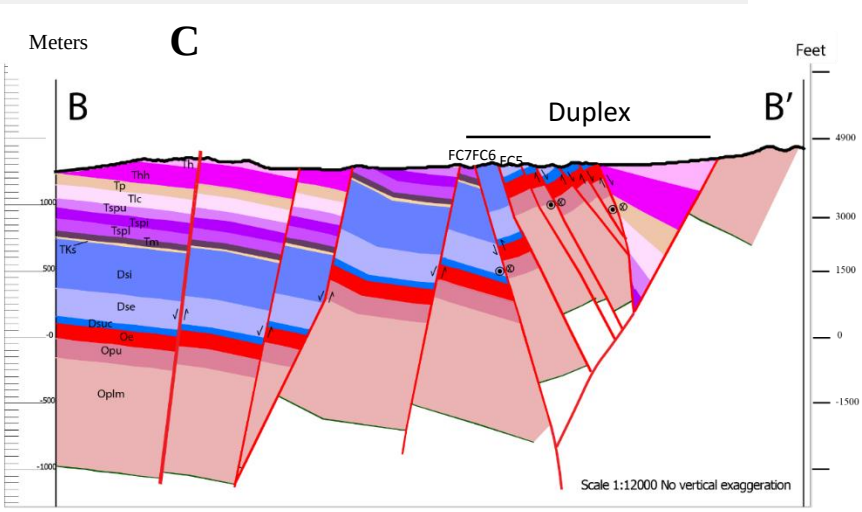

Figure 23.Explains coexisting reverse faults within extensional regions.
A: Geologic map shows locations of faults FC4, FC5, FC6, and FC7. Also, it displays tilting and rotation as the strike of the bedding changes in the vicinity of faults, FC4, FC5, FC6, and FC7. B1. 2D model shows final stage of the formation of the apparent reverse faults in a normal fault system. B2: 2D model that explains stages in formation of the reverse fault among the normal faults (After Fossen, 2010). Notice that with time as the beds are tilted and rotated, the faults which formed as a normal will become revers faults. C. Geologic cross-section BB' shows the duplex structure containing both normal and apparent reverse faults.

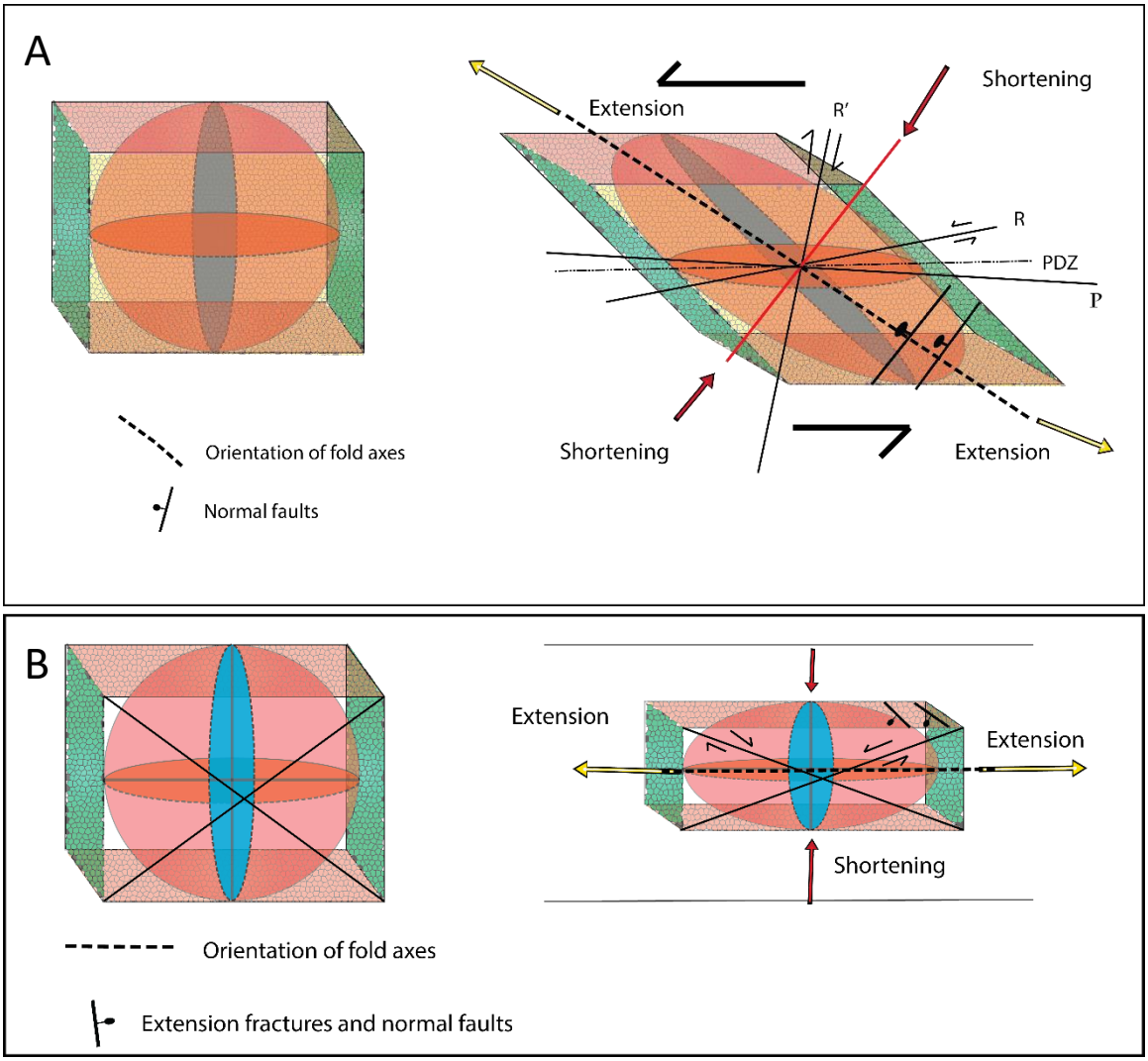

Figure 24. Strain ellipsoid of strike-slip deformation modified from Sylvester (1988).
A. Explains simple shear deformation and its associated structures. R and R' are synthetic and antithetic shears, respectively; P is a secondary fracture that may have synthetic shear; PDZ = principal displacement zone. B. Explains pure shear deformation and its associated structures.

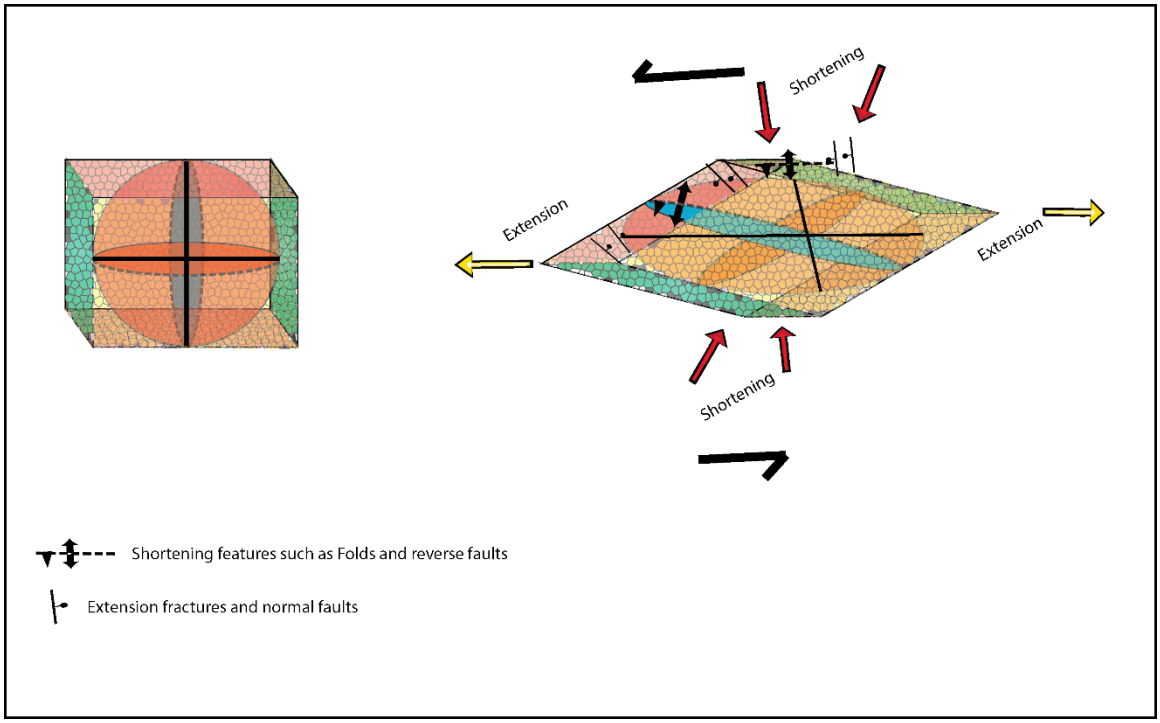

Figure 25. Schematic ellipsoid model explains a combination of the simple and pure shear deformations. Notice: This model might only apply to the duplex zone (restricted region).

APPENDICES

APPENDIX A

PLATES

Plate 1. Geologic map of the Maynard Lake fault and northwest Sheep Range, Lincoln County, Nevada, USA. (Please find the attachment entitled Geologic Map of MLF)

Plate 2. Geologic cross-sections of some parts of Maynard Lake fault zone.
(Please find Plate 2 in the attachment entitled Geologic Cross-sections of MLF)

APPENDIX B
Tables

Table 1. Calculated heave and throw of faults

Fault Name	Fault strike set	Slip Type	Domain	Throw	Heave	dip angle and direction
FN1	ENE	Normal slip	B	38.07 m	7.25 m	75W
FN2	ENE	Normal oblique-slip	B	74.86 m	26.37 m	70W
FB1(FN7)	Duplex fault	Reverse oblique slip	B	236.70 m	70.04 m	74 E
FN4	ENE	Normal dip-slip	B	277.16 m	5.49 m	85 W
FN5	N-S	Normal oblique-slip	B	129.26 m	60.21 m	65 W
FN6	N-S	Normal oblique-slip	B	97.68 m	69.11 m	54 W
FB2	Duplex fault	Normal oblique slip	A	1171.03 m	541.00 m	65 E
FC2	Duplex fault	Normal dip slip	A	32.38 m	22.26 m	55 E
FC3	Duplex fault	Normal oblique slip	A	30.87 m	23.28 m	53 E
FC4	Duplex fault	Normal oblique slip	A	106.76 m	58.69 m	61 E
FC5	Duplex fault	Normal dip slip	A	6.47 m	2.77 m	66 E
FC6	Duplex fault	Reverse oblique slip	A	384.17 m	199.32 m	63 E
FS3	NW	Normal dip-slip	C	9.14 m	1.65 m	80 W
FS4	N-S	Normal dip-slip	C	1571.54 m	92.67 m	85 E
FS5	N-S	Normal oblique-slip	C	495.24 m	96.12 m	79 W
FS6	N-S	Normal oblique-slip	C	171.28 m	62.41 m	70 W

Table 2. Major fold data

Fold Name	Domain	Type	Trend, plunge of fold axis	Strike and dip of Axial plane	Inter-limb angle	Class
A	B	syncline	052.2, 06.7	232.2, 89.6 N	164.6^{o}	gentle
B	B	anticline	284.2, 01.6	277.9, 14.3 N	155.4^{o}	gentle
C	B	syncline	058.0, 29.3	041.0, 62.5 E	138^{o}	gentle
D	B	syncline	329.7, 14.3	321.5, 60.7 E	113.2^{o}	open
E	B	antilcine	341.3, 01.8	340.7, 71.3 E	151.7^{o}	gentle
FDC1	A	syncline	339.9, 14.4	338.9, 86.0 E	120.4°	gentle
FDC2	A	anticline	233.3, 20.4	178.3, 24.4 W	155^{o}	gentle
FDS1	A	Syncline	037.0, 04.0	220.1, 53.1 W	123.5°	gentle

Table 3. Minor fold data

X	Y	fold name	Axial plan, strike	Axial Plan, dip	Dip direction	Hingline trend	Hingline plunge	interlimbangle	Class
-115.138	37.13389	e1	114.64	64.4	S	115.6	2	135	gentle
-115.138	37.13389	e2	96.9	81.8	S	98.3	9.8	139.4	gentle
-115.138	37.13427	f1	172.2	41.1	w	324.4	22.1	137.5	gentle
-115.138	37.13427	f2	67.6	70.1	S	70	6.5	142.2	gentle
-115.145	37.12062	g	56.8	11.5	S	187.5	8.8	139.5	gentle
-115.146	37.12043	h	13.8	18.8	E	18.7	1.7	114.1	gentle
-115.146	37.12099	i	41.9	16.6	E	194.7	7.8	111.3	open
-115.146	37.11985	j	1.8	10.2	E	10.1	1.5	161.4	open
-115.145	37.1209	k	35.1	16.7	E	195.8	5.7	149.3	gentle

Table 4. Mean vector of strike of compaction foliations

Mean strike compaction foliation cluster	East	Center	West	*Number of entries east to west respectively
Hiko Tuff	275 ± 13	348 ± 13	307 ± 18	8, 19, and 14
Harmony Hills Tuff	280 ± 18	352 ± 11	331 ± 8	9, 25, and 26
Shingle Pass Formation	327 ± 8	360 ± 16	341 ±10	22, 12, and 9

*represents number of strike and dip of compaction foliation taken from different tuffs

REFERENCES

Abdelhaleem, S.A., 2015 Kinematics and timing of the Miocene-Quaternary deformation in Nellis Dunes Recreational Area, Nevada, [M.S. thesis]: Las Vegas, Nevada, University of Nevada.73pp.

Allmendinger, R.W., Marrett, R.A., and Cladouhos, T., 2005, Stereonet v. 9.2.0: A program for analyzing geologic structures data. © R. W. Allmendinger, 2006-2014.

Anderson, E.M., 1905, The dynamics of faulting: Transactions of the Edinburgh Geological Society, v. 8, p. 387–402.

Anderson, E.M., 2012, The Dynamics of Faulting by E. M. Anderson: Geological Society, London, Special Publications, v. 367, p. 231–246, doi: 10.1144/SP367.16.

Anderson, R.E., compiler, 1999a, Fault number 1122, Maynard Lake fault, in Quaternary fault and fold database of the United States: U.S. Geological Survey website, http://earthquakes.usgs.gov/hazards/qfaults, accessed 04/03/2014.

Anderson, R.Ernest, compiler, 1999b, Fault number 1115, Sheep Basin fault, in Quaternary fault and fold database of the United States: U.S. Geological Survey website, http://earthquakes.usgs.gov/hazards/qfaults, accessed 08/07/2014.

Anderson, R.E., compiler, 1999c, Fault number 1121, Coyote Spring fault, in Quaternary fault and fold database of the United States: U.S. Geological Survey website, http://earthquakes.usgs.gov/hazards/qfaults, accessed 05/06/2016.

Anderson, R.E., Felger, T.J., Diehl, S.F., Page, W.R., and Workman, J.B., 2010, Integration of tectonic, sedimentary, and geohydrologic processes leading to a small-scale extension model for the Mormon Mountains area north of Lake Mead, Lincoln County, Nevada: Geological Society of America Special Paper 463, p. 395–426, doi: 10.1130/2010.2463(18).

Atwater, T., 1971, Implications of Plate tectonics for the Cenozoic Tectonic Evolution of Western North America: Geological Society of America Bulletin, v. 81, p. 3513–3536.

Axen, G.J., 1993, Ramp-flat detachment faulting and low-angle normal reactivation of the Tule Springs thrust, southern Nevada: Geological Society of America Bulletin, v. 105, p. 1076–1090, doi: 10.1130/0016-7606(1993)105<1076:RFDFAL>2.3.CO;2.

Axen, G.J., Taylor, W.J., and Bartley, J.M., 1993, Space-time patterns and tectonic controls of Tertiary extension and magmatism in the Great Basin of the western United States: Geological Society of America Bulletin, v. 105, p. 56–76, doi: 10.1130/0016-7606(1993)105<0056:STPATC>2.3.CO;2.

Becker, A., 1995, Conical drag folds as kinematic indicators for strike-slip fault motion: Journal of Structural Geology, v. 17, p. 1497-1503, doi: 10.1016/0191-8141(95)00057-K.

Best, M., Christiansen, E.H., Deino, A.L., Gromme, S., Hart, G.L., and Tingey, D.G., 2013a, The 36 – 18 Ma Indian Peak – Caliente ignimbrite field and calderas , southeastern Great Basin , USA : Multicyclic super-eruptions: Geosphere, v. 9, p. 864-950, doi: 10.1130/GES00902.1.

Best, M.G., 1988, Early Miocene change in direction of least principal stress, southwestern United States: Conflicting inferences from dikes and metamorphic core-detachment fault terranes: Tectonics, v. 7, p. 249–259, doi: 10.1029/TC007i002p00249.

Best, M.G., and Christiansen, E.H., 1991, Limited extension during peak Tertiary volcanism, Great Basin of Nevada and Utah: Journal of Geophysical Research: Solid Earth, v. 96, p. 13509–13528, doi: 10.1029/91JB00244.

Best, M.G., Gromme, S., Deino, A.L., Christiansen, E.H., Hart, G.L., and Tingey, D.G., 2013, The 36-18 Ma Central Nevada ignimbrite field and calderas, Great Basin, USA: Multicyclic super-eruptions: Geosphere, v. 9, p. 1562–1636, doi: 10.1130/GES00945.1.

Best, M.G., Scott, R.B., Rowley, P.D., Swadley, W.C., Anderson, R.E., Grommé, C.S., Harding, A.E., Deino, A.L., Christiansen, E.H., and Tingey, D.G., 1993, Oligocene-Miocene caldera complexes, ash-flow sheets, and tectonism in the central and southeastern Great Basin: Crustal evolution of the Great Basin and the Sierra Nevada. Geological Society of America Field Trip Guidebook, p. 285–312.

Bidgoli, T.S., 2005, the role of transverse faults in Great Basin extension: Transfer faults or N-S extension? [M.S. thesis]: Las Vegas, Nevada, University of Nevada, 111 pp

Bidgoli, T.S., Stockli, D.F., and Walker, J.D., 2015, Low-temperature thermochronologic constraints on the kinematic histories of the Castle Cliffs, Tule Springs, and Mormon Peak detachments, southwestern Utah and southeastern Nevada: Geosphere, v. 11, p. 850–867, doi: 10.1130/GES01083.1.

Byron, B., 1995, Local contraction along the Pahranagat Shear System, Southeastern Nevada: U.S. Geological Survey Bulletin, v. 2153, p. 253–264.

Camilleri, P. A., Yonkee, A, Coogan, J., and DeCelles, P.G., 1997, Hinterland to foreland transect through the Sevier Orogen, northeast Nevada to north central Utah: structural style, metamorphism, and kinematic history of a large contractional orogenic wedge: Brigham Young University Geology Studies, v. 42, p. 297–309, http://medcontent.metapress.com/index/A65RM03P4874243N.pdf.

Colgan, J.P., Dumitru, T.A., and Miller, E.L., 2004, Diachroneity of Basin and Range extension and Yellowstone hotspot volcanism in northwestern Nevada: Geology, v. 32, p. 121, doi: 10.1130/G20037.1.

Colgan, J.P., Dumitru, T.A., Reiners, P.W., Wooden, J.L., and Miller, E.L., 2006, Cenozoic tectonic evolution of the Basin and Range Province in northwestern Nevada: American Journal of Science, v. 306, p. 616–654, doi: 10.2475/08.2006.02.

Cook, E.F., 1965, Stratigraphy of Tertiary volcanic rocks in eastern Nevada: Nevada. Bureau of Mines Report 11, Mackay School of Mines, University of Nevada, 61 pp.

Dickinson, W.R., 2006, Geotectonic evolution of the Great Basin: Geosphere, v. 2, p. 353–368, doi: 10.1130/GES00054.1.

Dolgoff, A., 1963, Volcanic stratigraphy of the Pahranagat area, Lincoln County, southeastern Nevada: Geological Society of America Bulletin, v. 74, p. 875–900.

Dubey, A.K., 2014, Understanding an Orogenic Belt: Cham, Springer International Publishing, 401 p., doi: 10.1007/978-3-319-05588-6.

E.B. Ekren, R.C. Bucknam, W.J. Carr, G.L. Dixon, and W.D.Q., 1976, East-Trending Structural Lineaments in Central Nevada: UNITED STATES GOVERNMENT PRINTING OFFICE, WASHINGTON, p. 16, https://pubs.er.usgs.gov/publication/pp986?currow=1372.

Ekren, E.B., Orkild, P.P., Sargent, K.A., and Dixon, G.L., 1977, Geologic map of Tertiary rocks, Lincoln county, Nevada: U.S. Geological Survey Miscellaneous Investigations Series, Map I-1014, 1:250,000 scale, http://pubs.er.usgs.gov/publication/i1041.

Evans, M., 2016, Structural development and tectonic role of the Arrowhead Mine Fault, Pahranagat Shear Zone, Nevada, [M.S. thesis in progress]: Las Vegas, Nevada, University of Nevada.

Faulds, J.E., and Varga, R.J., 1998, the role of accommodation zones and transfer zones in the regional segmentation of extended terranes: Geological Society of America Special Papers, 323, p. 1–45, doi: 10.1130/0-8137-2323-x.1.

Fossen, H., 2010, Structural geology: Cambridge University Press, 457 pp.

Gibson, H.D., Walsh, J.J., Watterson, J., 1989. Modelling of bed contours and cross-sections adjacent to planar normal faults. Journal of Structural Geology, v. 11, p. 317–328.

Grasemann, B., Stu¨we, K., Vannay, J.-C., 2003. Sense and non-sense of shear in flanking structures. Journal of Structural Geology, v. 25, p. 19–34.

Grasemann, B., Martel, S., and Passchier, C., 2005, Reverse and normal drag along a fault: Journal of Structural Geology, v. 27, p. 999–1010, doi: 10.1016/j.jsg.2005.04.006.

Guth, P.L., 1981, Tertiary extension north of the Las Vegas Valley shear zone , Sheep and Desert Ranges , Clark County , Nevada: Geological Society of America Bulletin, v. 92, p. 763–771.

Guth, P.L., 1990, Superposed Mesozoic and Cenozoic deformation, Indian Springs quadrangle, southern Nevada: Geological Society of America Memoirs, v. 176, p. 237–250.

Hague, Arnold, 1883, Abstract of report on the geology of the Eureka district, Nevada: U. S. Geol. Survey 3d annual report., p. 237-272.

Hamblin, W.K., 1965. Origin of ‘reverse drag’ on the down-thrown side of normal faults. Geological Society of America Bulletin, v.76, p. 1145–1164.

Hammond, W.C., and Wayne Thatcher, 2005, Northwest Basin and Range tectonic deformation observed with the Global Positioning System, 1999–2003: Journal of Geophysical Research, v. 110, p. B10405, doi: 10.1029/2005JB003678.

Harding, A.E., Robert B. Scott, Harald H. Mehnert, and Lawrence W. Snee, 1992, Evidence of the Kane Springs Wash Caldera in the Meadow Valley Mountains, Southeastern Nevada: U.S. geological survey bulletin 2056--E, p. U.S. Geological Survey Bulletin 2056–E, 135–179.

Henry, C.D., 2008, Ash-flow tuffs and paleovalleys in northeastern Nevada: Implications for Eocene paleogeography and extension in the Sevier hinterland, northern Great Basin: Geosphere, v. 4, p. 1, doi: 10.1130/GES00122.1.

Hudson, M.R., Rosenbaum, J.G., Gromme, C.S., Scott, R.B., and Rowley, P.D., 1998, Paleomagnetic evidence for counterclockwise rotation in a broad sinistral shear zone, Basin and Range province,

southeastern Nevada and southwestern Utah: Geological Society of America Special Paper 323, p., p. 149–180.

Hudson, M.R., Rosenbaum, J.G., Scott, R.B., and Rowley, P.D., 1995, Palemagnetic data from the Miocene Hiko Tuff, southeastern Nevada, and their tectonic implications: US Geological Survey Bulletin, v. 2056, p. 219–232.

Hudson, M.R., Sawyer, D.A., and Warren, R.G., 1994, Paleomagnetism and rotation constraints for the middle Miocene southwestern Nevada volcanic field: Tectonics, v. 13, p. 258–277, doi: 10.1029/93TC03189.

Jayko, A.S., 1990, Shallow crustal deformation in the Pahranagat area, southern Nevada: Geological Society of America Memoir 176, p. 213–236.

Jayko, A.S., 2007, Geologic Map of the Pahranagat Range 30’ x 60' Quadrangle, Lincoln and Nye Counties, Nevada: United States Geological Survey Scientific Investigations Map 2904, 1:100,000 scale, http://pubs.usgs.gov/sim/2007/2904/.

Jones, C.H., Wernicke, B.P., Farmer, G.L., Walker, J.D., Coleman, D.S., McKenna, L.W., and Perry, F.V., 1992, Variations across and along a major continental rift; an interdisciplinary study of the Basin and Range Province, Western USA: Tectonophysics, v. 213, p. 57-96.

King, G.C.P., Stein, R., Rundle, J., 1988. The growth of geological structures by repeated earthquakes, 1: conceptual framework. Journal of Geophysical Research 93, 13307–13318.

Kreemer, C., Blewitt, G., and Bennett, R.A., 2010, Present-day motion and deformation of the Colorado Plateau: Geophysical Research Letters, v. 37, p. 1-5.

Kneissl, T., Van Gasselt, S., and Neukum, G., 2010, Measurement of strike and dip of geologic layers from remote sensing data---New software tool for ArcGIS: Lunar and Planetary Science Conference, v. 41, p. 1640.

Liggett, M.A., and Ehrenspeck, H.E., 1974, Pahranagat shear system, Lincoln County, Nevada: U.S. National Aeronautics and Space Administration Report CR-136388, 10 pp.

Liu, M., 2001, Cenozoic extension and magmatism in the North American Cordillera: the role of gravitational collapse: Tectonophysics, v. 342, p. 407–433, doi: 10.1016/S0040-1951(01)00173-1.

Liu, M., and Shen, Y., 1998, Crustal collapse, mantle upwelling, and Cenozoic extension in the North American Cordillera: Tectonics, v. 17, p. 311–321, doi: 10.1029/98TC00313.

Long, S.P., 2012, Magnitudes and spatial patterns of erosional exhumation in the Sevier hinterland, eastern Nevada and western Utah, USA: Insights from a Paleogene paleogeologic map: Geosphere, v. 8, p. 881–901, doi: 10.1130/GES00783.1.

Ma, X.Q., Kusznir, N.J., 1993. Modelling of near-field subsurface displacements for generalized faults and fault arrays. Journal of Structural Geology, v. 15, p. 1471–1484.

Piety, B.L.A., 1996, Compilation of known or suspected Quaternary faults within 100 km of Yucca Mountain, Nevada and California: US Geological Survey Open-File Report 94-112,404 pp., http://www.osti.gov/scitech/biblio/463573.

Price, T.P., 2016, Investigating OligoceneMiocene folded tuffs and extensional faults along the Buckhorn fault, Pahranagat shear zone, Nevada, [M.S. thesis in progress]: Las Vegas, Nevada, University of Nevada.

Rau, C.J., and Forsyth, D.W., 2011, Melt in the mantle beneath the amagmatic zone, southern Nevada: Geology, v. 39, p. 975–978, doi: 10.1130/G32179.1.

Reso, A., 1963, Composite columnar section of exposed Paleozoic and Cenozoic rocks in the Pahranagat Range, Lincoln County, Nevada: Geological Society of America Bulletin, v. 74, p. 901–918.

Rowley, P.D., 1998, Cenozoic transverse zones and igneous belts in the Great Basin, western United States: Their tectonic and economic implications Geological Society of America Special Paper 323, p., p. 195–228.

Schlische, R.W., 1995, Geometry and origin of fault-related folds in extensional settings: American Association of Petroleum Geologists Bulletin, v. 79, p. 1661–1678, doi: 10.1306/7834DE4A-1721-11D7-8645000102C1865D.

Scott, R.B., Gromme, C.S., Best, M.G., Rosenbaum, J.G., and Hudson, M.R., 1992, Stratigraphic relationships of Tertiary volcanic rocks in central Lincoln County, southeastern Nevada: Geologic studies in the Basin and Range—Colorado Plateau transition in southeastern Nevada, southwestern Utah, and northwestern Arizona, U.S. Geological Survey Bulletin 2153, p. 5–42.

Scott, R.B., Unruh, D.M., Snee, L.W., Harding, A.E., Nealey, L.D., Jr, H.R.B., and Budahn, J.R., 1995, Relation of peralkaline magmatism to heterogeneous extension during the middle Miocene, southeastern Nevada: American Geophysical Union, v. 100, p. 10381–10401, http://onlinelibrary.wiley.com/doi/10.1029/94JB03217/full.

Sonder, L.J., and Jones, C.H., 1999, WESTERN UNITED STATES EXTENSION: How the West was Widened: Annual Review of Earth and Planetary Sciences, v. 27, p. 417–462, doi: 10.1146/annurev.earth.27.1.417.

Stewart, J., 1998, Regional characteristics, tilt domains, and extensional history of the later Cenozoic Basin and Range Province, western North America: Geological Society of America Special Paper323, p. 47-74.

Stewart, J.H., 1980, Regional tilt patterns of late Cenozoic basin-range fault blocks, western United States: Geological Society of America Bulletin, v. 91, p. 460-464, doi: 10.1130/0016-7606(1980)91<460:RTPOLC>2.0.CO;2.

Sylvester, A.G., 1988, Strike-slip faults: Geological Society of America Bulletin, v. 100, p. 1666–1703, doi: 10.1130/0016-7606(1988)100<1666:SSF>2.3.CO;2.

Tschanz, C.M., and Pampeyan, E.H., 1970, Geology and mineral deposits of Lincoln County, Nevada: Nevada Bureau of Mines, Bulletin 73, 188 pp.

Taylor, W.J., and Bartley, J.M., 1992, Prevolcanic extensional Seaman breakaway fault and its geologic implications for eastern Nevada and western Utah: Geological Society of America Bulletin, v. 104, p. 255–266, doi: 10.1130/0016-7606(1992)104<0255:PESBFA>2.3.CO;2.

Taylor, W.J., and Switzer, D.D., 2001, Temporal changes in fault strike (to 90°) and extension directions during multiple episodes of extension: An example from eastern Nevada: Geological Society of America Bulletin, v. 113, p. 743–759, doi: 10.1130/0016-7606(2001)113<0743:TCIFST>2.0.CO;2.

Taylor, W.J., Bartley, J.M., Lux, D.R., and Axen, G.J., 1989, Timing of Tertiary extension in the Railroad Valley-Pioche Transect, Nevada: Constraints from 40 Ar/ 39 Ar ages of volcanic rocks: Journal of Geophysical Research, v. 94, p. 7757, doi: 10.1029/JB094iB06p07757.

Taylor, W.J., Bartley, J.M., Martin, M.W., Geissman, J.W., Walker, J.D., Armstrong, P.A., and Fryxell, J.E., 2000, Relations between hinterland and foreland shortening: Sevier orogeny, central North American Cordillera: Tectonics, v. 19, p. 1124–1143, doi: 10.1029/1999TC001141.

Wells, M.L., Hoisch, T.D., Cruz-Uribe, A.M., and Vervoort, J.D., 2012, Geodynamics of synconvergent extension and tectonic mode switching: Constraints from the Sevier-Laramide orogen: Tectonics, v. 31, 20 pp. n/a–n/a, doi: 10.1029/2011TC002913.

Wernicke, B., Axen, G.J., and Snow, J.K., 1988, Basin and Range extensional tectonics at the latitude of Las Vegas, Nevada: Geological Society of America Bulletin, v. 100, p. 1738–1757, doi: 10.1130/0016-7606(1988)1002.3.CO;2.

Wernicke, B., 1992, Cenozoic extensional tectonics of the US Cordillera: The Geology of North America, v. 3, p. 553–581.

Wernicke, B., and Snow, J.K., 1998, Cenozoic tectonism in the Central Basin and Range: Motion of the Sierran-Great Valley block: International Geology Review, v. 40, p. 403–410, doi: 10.1080/00206819809465217.

Zoback, M. Lou, 1989, State of stress and modern deformation of the Northern Basin and Range Province: Journal of Geophysical Research, v. 94, p. 7105, doi: 10.1029/JB094iB06p07105.

Zoback, M. Lou, Anderson, R.E., and Thompson, G.A., 1981, Cainozoic evolution of the state of stress and style of tectonism of the Basin and Range province of the western United States: Philosophical Transactions of the Royal Society of London. Series A, Mathematical and Physical Sciences, v. 300, p. 407–434, doi: 10.1098/rsta.1981.0073.

CURRICULUM VITAE

Mahmud Muhammad

Degree

Bachelor of Science, Geology, 2010
Salahaddin University, Erbil, Kurdistan Region-Iraq

Awards

2016 Edwards & Olswang Geology Scholarship (provided by the University of Nevada Las Vegas-Geoscience Department.

2015 The Nevada Petroleum & Geothermal Society (NPGS).

2015 U.S. Geological Survey EdMap student designated in award No. G15AC00157

2013 Iraqi Scholars and Leaders Program funded by Exxon Mobil.

Publications

Mahmud M. Muhammad and Abdullah H. Awdal, Automatic Mapping of Lineaments Using Shaded Relief Images Derived from Digital Elevation Model (DEM) in Erbil-Kurdistan, northeast Iraq, ANAS Volume 6, Number 2: January-March, 2012 pages (138-146).

Mahmud Muhammad and W. J. Taylor, 2016, Structural evolution of the Maynard Lake Fault (MLF) within the left-lateral Pahranagat shear zone (PSZ), Nevada, USA. in Geological Society of America Abstracts with Programs, v 48, no. 4, paper no. 15-1, doi: 10.1130/abs/2016CD-274230.

Affiliation

Secretary of the UNLV AAPG student chapter August 2015-March 2016

Geological Society of America (GSA) member since 2014

American Association of Petroleum Geologists (AAPG) member since April 2012

Kurdistan Geologists syndicate member since November 2010

Thesis Title: Structural Evolution of the Maynard Lake fault (MLF) within the left-lateral Pahranagat shear zone (PSZ), Nevada, USA.